Metabolic Studies of Hepatic Response to Diabetes Drugs

A Thesis Submitted by

Katherine Carson

In partial fulfillment of the requirements for the degree of

Master of Science

In Chemical Engineering

TUFTS UNIVERSITY

November, 2011

Abstract

A major concern in drug development is the potential for chemical injury to the liver. Drugs account for 1/3~1/2 of acute liver failures, yet underlying toxicity mechanisms are poorly understood. Adverse reactions are often detected too late, as with troglitazone, an antidiabetic drug introduced in 1997 and withdrawn in 2000 after several cases of liver failure. Predictions are more limited with multi-drug interactions, common among patients with chronic ailments like diabetes. Here we develop a microfluidic reactor for the culture of HepG2 cells and the establishment of a steady state drug gradient. Traditional in vitro experiments explore the metabolic effects of troglitazone on HepG2 cells and the interactions between rosiglitazone and metformin (common antidiabetic compounds). LC-MS methods are developed for the detection of drugs and key metabolites. This research expands our knowledge drug metabolism in the liver and introduces a physiologically relevant platform for the testing of drug interactions.

Acknowledgments

Thank you to my committee members, Dr. Daniel Ryder and Dr. Catherine Kuo, for making time for me at the last minute, for your patience in all your reorganizing, and for supporting me in research and thesis. Your kindness and commitment to my education are very much appreciated.

Thanks to all my incredible lab-mates: To Dr. Hai Shi, for training me in so very much and never showing any irritation when I asked yet another question (or the same one again!) His kindness, gentility, patience, and sheer volume of knowledge are rare. To Dr. Ning Lai, for her support and collaboration, but especially for her friendship – her presence in my first few years at Tufts means far more to me than I could ever write here. Ning is the stuff the very best friends are made of. To Gautham, for supporting me so generously with his time and his energy when I had run out of my own. It has been inspiring to witness his growth as a grad student and researcher and I feel lucky to work beside him. To James, for his energetic and proactive spirit, for finding and fixing all the myriad little things wrong with our lab, for keeping the place neat and tidy, and for his good company and sympathetic support on long days. To Meenal, for the companionship. To Julie, and Joanna, for being such good-natured new labmates. To Mike and Kim for all the incredible grunt work carried out so cheerfully, and to all my other friends in the department, especially Brian, Ann, Beth, Jenny, Andrew, Amy, Ciuxian, and Yanping and Christina, for everything.

Thank you to my incredible family who supported me through this long process, from my own parents and brother who listened to all my gripes, cheered me on when I

was sure I was out of steam, and even took charge of my daughter to help me finish this thesis. To my husband's parents who offered their own words of experience and support (as biology PhDs themselves). To Elsie, who cheers me up with each and every smile – who makes life wonderful. Special thanks to my husband, Evan, for putting up with his grad-student wife and for being the stable and incredibly supportive spouse that he is, for holding a "real job" while I indulge in academia, for being a family man, and for doing it all when I cannot.

Most of all, I would like to thank my advisor, Dr. Kyongbum Lee, for years of unfaltering support and invaluable teaching. Under his guidance, I have learned to ask questions, solve problems, analyze critically, and act independently in a ways I never believed that I could. He has truly changed the way I think, whether or not I ever get a PhD. All this with the most trusting and respectful manner I have observed in any PI. I don't know if he ever doubted me (couldn't blame him: I doubt me all the time), but if he did, he never let me feel it. I consider myself extremely fortunate to have fallen into his group. I might not have finished any degree at all for anyone else. Thank you, Professor Lee. You are truly a model of effective and kind advising.

Contents

List of Figures

List of Tables

Metabolic Studies of Hepatic Response to Diabetes Drugs

Chapter 1: Introduction

Diabetes

In a healthy person, consuming food leads to a spike in blood glucose levels, which triggers insulin production by beta cells in the islets of Langerhans of the pancreas. Insulin stimulates liver and skeletal muscle cells to take up glucose for immediate use or for storage as glycogen (glycogenesis). This process depletes blood glucose, and the body returns to its fasting state. The decrease in blood glucose reduces insulin production by beta cells, while increasing glucagon production by alpha cells in the islets of Langerhans. In the fasted state, glucagon breaks down the glycogen stores to produce glucose (glycogenolysis) and feeds cellular metabolism in the body. Glycogenolysis continues until the body is either fed again or the glycogen stores are exhausted. If fasting continues for a prolonged period of time (beyond a day), glucose is synthesized in the liver from non-carbohydrate substrates such as lactate, glycerol, and amino acids (gluconeogenesis). Similar to glycogenolysis, gluconeogenesis is stimulated by glucagon.

Diabetes disrupts the insulin-mediated cellular uptake of glucose, leading to a loss of control over the blood glucose level. Diabetes occurs in two forms. In type I diabetes, insulin production is inadequate and must be supplemented. In type 2 diabetes (also called *non-insulin dependent diabetes* or *adult-onset diabetes*), insulin production is sufficient, but ineffective due to the loss in sensitivity of the body to the hormone

(Memmler et al. 1999). The loss of insulin sensitivity imposes a permanent, false fasting state, where glycogenolysis and gluconeogenesis continue to occur under fed conditions. The continued production of glucose is compounded by the lack of glucose absorption, leading to chronic elevation of blood glucose (hyperglycemia). To compensate for the loss in insulin sensitivity, the pancreas increases the production of insulin, leading to an excess level of insulin in the blood circulation (hyperinsulinemia).

The loss in control over blood glucose is devastating to the body, and can lead to a number of pathological consequences. On the one hand, cells that cannot access glucose behave as though starved. Neurons are particularly vulnerable to this sugar starvation as they rely on glucose as a form of rapidly metabolized energy for proper function. Numbness of the extremities is common. In long-term cases, blindness and coma can result. In addition, adipocytes do not take up and free fatty acid from the bloodstream as in a healthy individual, so lipid levels rise in the blood (hyperlipidemia), often leading to gall stones as the cholesterols crystalize at high concentrations, and eventually leading to heart disease and kidney failure. On the other hand, the blood is in a perpetually hyperglycemic state, awash with sugars. This puts additional strain on the kidneys, which work to excrete the excess sugar whole. Osmosis drives water into the sugary urine and dehydrates the body. High levels of glucose leave interstitial fluid spaces highly susceptible to bacterial infection. The risk of infections from wounds is also increased due to the depressed function of the nervous system and the resulting numbness of the extremities. (Thibodean 2002)

Diabetes is a rapidly growing problem in the United States. The Center for Disease Control estimates that 25.8 million people, 8.3% of the American population, are

diabetic. Type 2 diabetes comprises the vast majority of these cases, 90-95%. A staggering 79 million Americans over the age of 20 (35% of that population) are thought to have prediabetes, making them highly susceptible to developing type 2 diabetes later in life. (CDC, 2011)

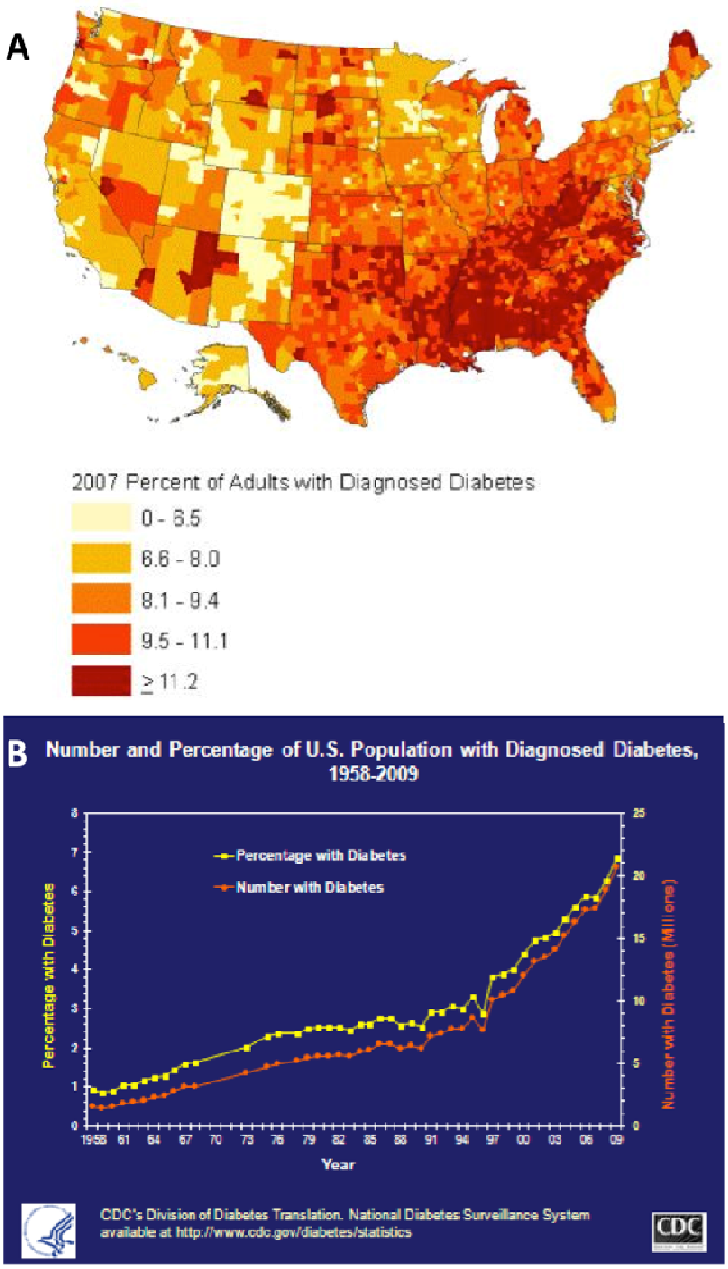

Figure 1: Diabetes Statistics

Figure 1: (A) The Diabetes Belt. Prevalence is especially high across the South East of the United States. (Barker et al. 2011) (B) Diabetes rates over the past half-century. Both instance and rate of increase have accelerated. (CDC)

The problem is not only American. A conservative projection predicts 366 million cases of diabetes globally by the year 2030. It should be noted that this projection is based on year 2000 statistics (171 million cases) assuming no further increase in rates of obesity. (Wild et al. 2004) This projection is likely an underestimate, as obesity rates have also been accelerating over the last three decades. The International Diabetes Federation estimates 285 million cases of diabetes worldwide, and projects 438 million by 2030. (International Diabetes Federation, 2009)

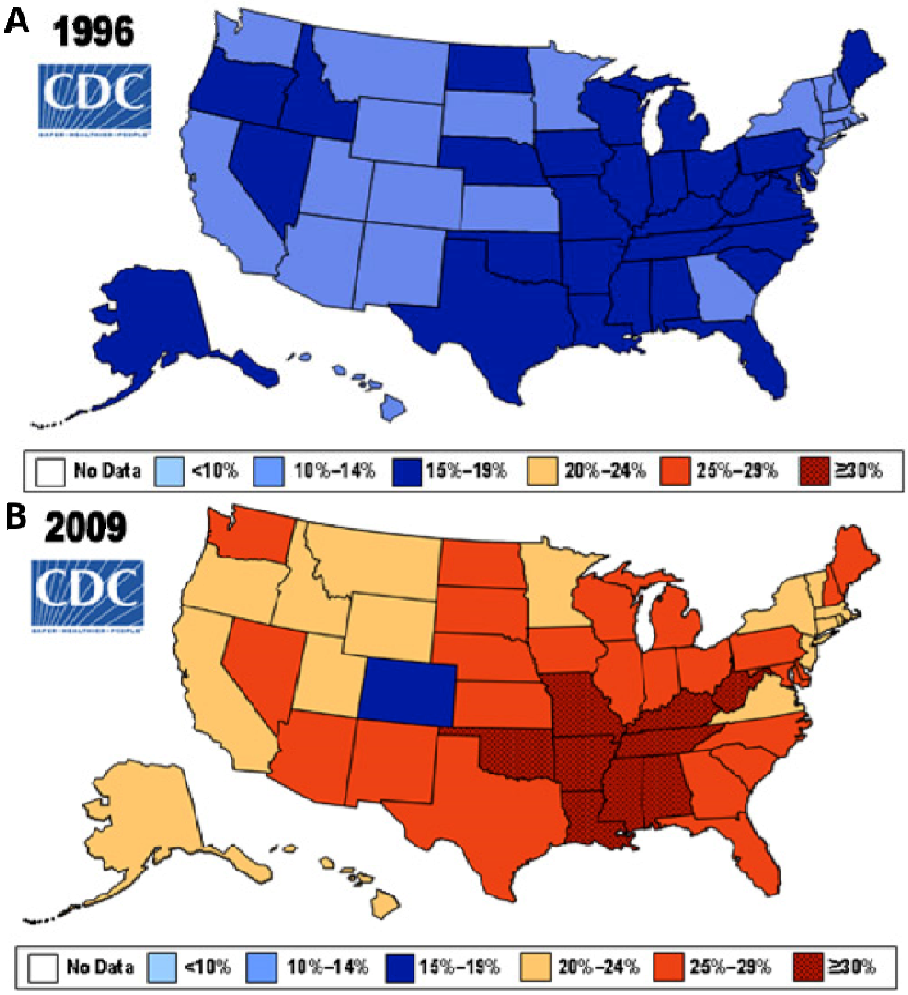

Figure 2: Obesity Rates in The United States

Figure 2: Obesity rates by state in (A) 1996 and (B) 2009. The highest prevalence occurs in the South East, similar to the Diabetes Belt in Figure 1. Taken from The CDC.

While lifestyle changes like exercise and healthy diet can and should be used to help prevent and treat type 2 diabetes (Gillies et al. 2007), a substantial and growing population requires medications as well. (American Diabetes Association 2009)

Drug Treatment of Diabetes

An important goal of drug treatment in type 2 diabetes is to restore control over blood glucose. Two representative orally administered drugs belong to the biguanide and thiazolidinedione (TZD) class of chemicals. The biguanides are used to lower blood glucose, whereas the TZDs are used to improve insulin sensitivity.

Metformin

Metformin, a biguanide, is often the first line of drug treatment for type 2 diabetes and the only drug recommended for preventing diabetes in high-risk patients. (American Diabetes Association 2009). Metformin is widely prescribed. In 2007, over 120 million people were taking metformin to control their blood glucose. (Towler et al. 2007)

Unlike most drugs, metformin does not undergo any chemical modification in the body. The kidneys secrete the drug unchanged. The exact mechanism for metformin's action remains unclear, but metformin is known to be an agonist for AMP-activated protein kinase (AMPK), which inhibits gluconeogenesis in the liver, thus lowering blood sugar levels. AMPK is more commonly turned on by a decrease in ATP that leads to a rise in ADP:ATP ratio, and an even greater increase in AMP:ATP ratio. Metformin may activate AMPK by increasing the amount of adenosine monophosphate (AMP) in the blood stream (Shang et al. 2007) or by affecting mitochondrial calcium levels (Kirpichnikov et al. 2002).

The drug is considered safe, though some worries about lactic acidosis remain due a rise in lactate production from the liver. If severe, lactic acidosis can significantly raise blood lactate to life-threatening levels. The reported instance of severe lactic acidosis is 5 cases per 100,000; however, all of these patients had other conditions such as heart

disease that predisposed them to lactic acidosis. (Misbin et al. 1998) The confounding influences of other underlying health problems present difficulties in isolating the effects of the drug and clearly establishing a causal role of Metformin in lactic acidosis. (Stades 2004)

Thiazolidinediones and Peroxisome Proliferator-Activated Receptors

Thiazolidinediones are the first class of synthetic compounds developed specifically to treat insulin resistance. (Yki-Järvinen 2004) The TZDs are ligands for peroxisome proliferator-activated receptors (PPARs), which act as nuclear hormone receptors as well as transcription factors. There are several isoforms of PPARs, with varying distributions across different tissue types. For example, PPAR-α is found predominantly in the liver. Its activation increases free fatty acid oxidation and controls the expression of genes that regulate lipoprotein concentration in the blood. Another isoform, PPAR-γ, is expressed mostly in adipose (fat) tissue. Activation of PPAR-γ is a key step in the differentiation program of adipocytes (fat cells). Indeed, PPAR-γ is considered a master regulator of adipogenesis, which refers to the formation of new adipocytes from fibroblast-like preadipocytes. Upon differentiation, adipocytes express higher levels of metabolic activity, especially glucose uptake and lipid synthesis (Barrick et al. 2005) The TZDs are strong agonists of PPAR-γ with affinities (dissociation equilibrium constants) in the nM range. (Masubuchi 2006).

There are two mechanisms for the agonist action (ligand activation): transactivation, which is DNA dependent, and transrepression, which is independent of DNA binding. In transactivation, TZD binds to the PPAR-γ, which acts with retinoid X receptor (RXR) and recruits coactivators to trigger transcription of PPAR target genes

through a DNA response element (peroxisome proliferator hormone response element, PPRE). In transrepression, TZD again forms a complex with PPAR-γ through ligand binding. The complex interferes negatively with other signal transduction pathways, preventing transcription of other target genes. (Yki-Järvinen 2004)

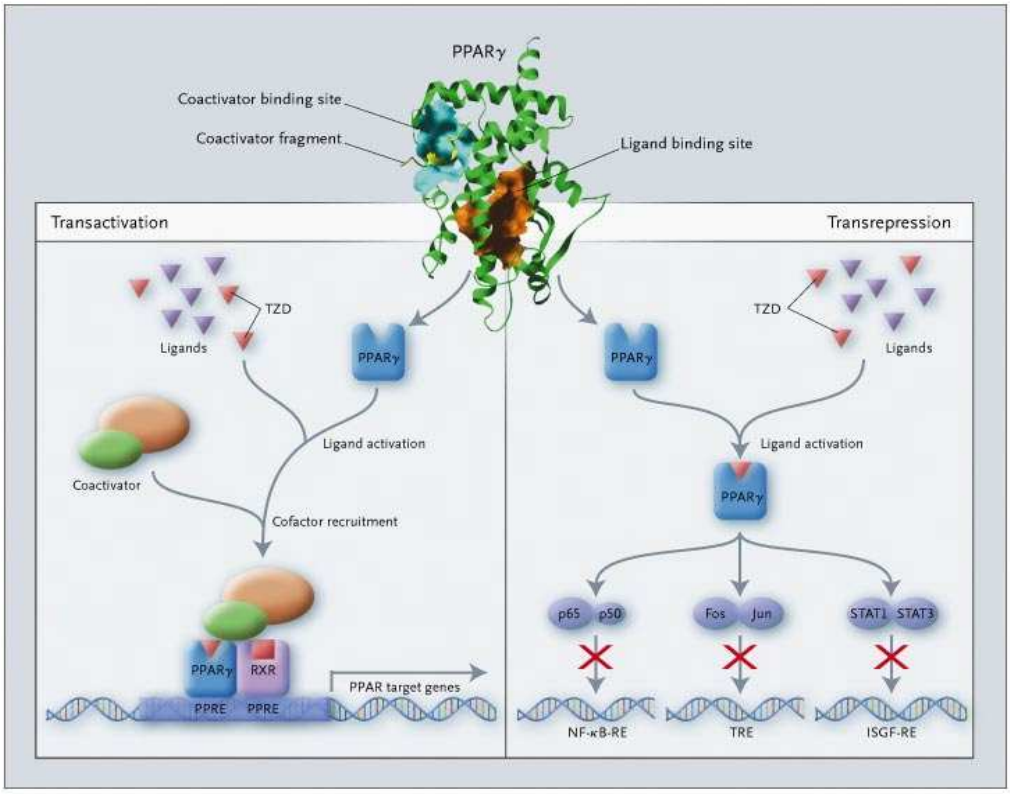

Figure 3: Molecular mechanisms of TZD

Figure 3: Molecular mechanisms of TZD action. In transactivation, the drug binds to PPAR-γ, forming a complex with coactivators and another ligand activated nuclear receptor, retinoid X receptor (RXR), to start transcription of PPAR target genes. It should be noted that ligand activated PPAR-γ can initiate transcription even without forming a complex with RXR. In transrepression, the ligand-PPAR-γ complex represses transcription of different target genes such as the targets of nuclear factor-κB (NF-κB),

interferon-stimulated gene factor (ISGF), and the phorbol ester 12-*O*-tetradecanoylphorbol 13-acetate (TPA). (Yki-Järvinen 2004)

At the whole-body level, treatment with TZD drugs promotes PPAR-γ mediated stimulation of adipogenesis, leading to an increase in the number of metabolically active adipocytes in adipose tissue depots. The increased metabolic capacity improves glucose uptake from the blood as well as the clearance and retention of free fatty acids through lipid synthesis and storage. It is not a surprise that a common side effect of these drugs is weight gain and increase in body fat mass. Though somewhat paradoxical, as excess body fat correlates strongly with the pathogenesis of type 2 diabetes, the clinical benefit of TZD drugs is explained by the increased capacity to store lipids in adipose tissue depots, which can prevent harmful ectopic storage of lipids in peripheral tissues while lowering blood glucose and fatty acid levels. For example, chronically elevated levels of blood glucose and free fatty acids lead to lipid deposits in the liver. Excessive accumulation of lipid droplets in liver parenchymal cells (hepatocytes) can cause various pathological conditions such as non-alcoholic fatty liver disease, cirrhosis, and organ failure.

To date, three TZDs have been marketed as drugs to treat type 2 diabetes. These are troglitazone (TGZ), rosiglitazone (ROSI), and pioglitazone (PIO). This thesis research concentrates on TGZ and ROSI. TGZ was released in 1997, but had to be withdrawn from the market abruptly in early 2000, after several cases of liver failure due to drug toxicity. Rosiglitazone remains in use, although very recent reports implicate ROSI with an increased risk of heart attacks (Food and Drug Administration, 2010;

Nissen et al. 2007). Pioglitazone is currently considered safe. Both ROSI and PIO are frequently prescribed in conjunction with metformin.

Drug Metabolism in the Liver

In hepatocytes, biotransformation of drugs and other xenobiotic compounds generally occurs in two phases. In phase I, non-synthetic reactions reduce, oxidize, or hydrolyze the drug, resulting in the addition of new functional groups. The redox reactions involve the transfer of electrons via carrier molecules and cofactors such as NADPH. Thus, the continued regeneration of NADPH from its oxidized form ($NADP^+$) via the pentose phosphate pathway and malate cycle is critical to the operation of phase I reactions (Lehinger et al. 1993; Henderson et al. 2003). In phase II, the chemicals functionalized by phase I reactions are further modified by synthetic conjugation reactions. Phase II reactions include glucuronidation, sulfation and methylation, as well as conjugation with amino acids, glutathione, and other small peptides (Tredger et al. 2002; Traber et al. 1989). Phase II biotransformation significantly increases the polarity (water solubility) and molecular weight of the xenobiotic. These modifications are crucial to the elimination of the reactive intermediates formed during phase I.

Glutathione (GSH) conjugation is especially important, because this reaction competes with the deactivation of free radicals and other reactive oxygen species (ROS). Normally, intracellular GSH concentrations are sufficient to detoxify even highly reactive compounds. However, a severe chemical challenge (e.g. from a drug overdose) may overwhelm this defense mechanism (Henderson et al. 2003). Conversely, drug elimination via glutathione conjugation may deplete the GSH pool and sensitize the hepatocyte to ROS damage. Replenishing the GSH pool through biosynthesis depends on

an adequate supply of the amino acid building blocks. The availability of cysteine and methionine are particularly important for maintaining GSH levels because they contain the thiol moiety required for GSH synthesis (Glazenburg et al. 1983). The reduced form of GSH may also be regenerated from the oxidized form (GSSG) via an NADPH-dependent GSH reductase.

The substrate and cofactor dependencies implied by biochemical considerations are consistent with experimental and computational studies on the metabolic effects of drug exposure in hepatocytes. For example, metabolic profiling experiments in HepG2 cells and primary human hepatocytes have shown that several biguanides with insulin sensitizing action (phenformin, buformin and metformin) induce respiratory inhibition and compensatory increases in lactate production from accelerated glycolysis (Dykens et al. 2008). Importantly, the extent of the metabolic compensation was consistent with *in vitro* cytotoxicty (Wang et al. 2003) as well as previously observed *in vivo* lactic acidosis. Indeed, phenformin and buformin have both been withdrawn from the market because of unacceptably high incidence of potentially-fatal lactic acidosis, whereas metformin, which causes the smallest metabolic disturbance, is associated with substantially less risk of lactic acidosis (Goodarzi et al. 2005). In another study, metabolic flux analysis of HepG2 cells exposed to diclofenac and tacrin, two drugs known to have an uncoupling effect, revealed significant changes in intermediary metabolism even at concentrations considerably below the EC_{50} values, including an increase in the TCA cycle flux (Niklas et al. 2009). Taken together, these findings suggest that changes in the cellular metabolic flux distribution could robustly capture significant drug effects.

In Vitro Drug Testing

A major concern in drug development is the potential for chemical injury to the liver, which is the major site of xenobiotic transformation in the body. Drugs have been estimated to account for 1/3~1/2 of acute liver failures (Tafazoli et al. 2005). Unfortunately, adverse reactions are often detected only after the drug has been released onto the market and not during development or clinical trials, let alone the discovery stage. Predicting hepatic damage during preclinical development is limited by incomplete knowledge of the underlying toxicity mechanisms (Grattagliano et al. 2009). Predictions are even more limited with multi-drug interactions, which are common among patients with chronic ailments such as diabetes. Animal based toxicity assays are too costly to support combinatorial testing. Moreover, the predictive power of these assays is limited, as hepatotoxicity has a poor concordance between different species (O'Brien et al. 2006). A complementary or even alternative approach to animal testing is to perform *in vitro* analyses using primary human hepatocytes and their cell line analogs such as HepG2 and HepaRG (Gripon et al. 2002; Hart et al. 2010), as drug biotransformation primarily occurs in the parenchymal cells of the liver, i.e. hepatocytes. Despite the time and resources devoted to such preliminary *in vitro* work, only 10% of drugs that pass these tests and enter Phase 1 clinical trials ultimately gain approval for release to the market (Milwoud et al. 2011). This leaves much room for improvement and specialization of *in vitro* platforms.

Conventionally, *in vitro* testing of drug candidates utilize hepatocytes cultured in multi-well plates or culture flasks. Cells are seeded into the relatively large container where they adhere to the flat plastic surface to grow in two dimensions. More advanced configurations use natural or synthetic substrates to coat the culture surface or

encapsulate the cells, which improves cell attachment and stabilizes differentiated cell function (Berthiaume et al; 1996). The chief benefit of the cell culture models is that hepatocyte-specific responses to drug exposure can be studied in isolation from confounding systemic influences. Other important benefits include ease of use and control over experimental conditions. On the other hand, significant limitations remain, including the lack of spatial control over the cellular microenvironment and the loss of physiological gradients that are present in the intact liver. Over the last two decades, increasingly sophisticated hepatocyte culture technologies have been developed to address these and other common limitations associated with conventional well-plate cell culture models.

One prominent approach to addressing the lack of gradients has been to use microfluidics. Microfluidic devices for cell culture are usually constructed from optically transparent, biocompatible materials such as polydimethylsiloxane (PDMS) or glass, in which channels on the order of 10^0 to 10^2 microns in width and depth have been etched or cast. These devices are used to manipulate small amounts of fluid (10^{-9} to 10^{-18} L). The device designs range from simple arrays of channels for pressure-driven flow to very complex networks with many layers and membranes and miniaturized mechanisms (Whitesides 2006). The small dimensions of microfluidic devices guarantee that flow within the channels is laminar ($Re < 2100$) for most biologically relevant fluids and flow velocities. Due to laminar flow, mass transport across the channels (perpendicular to the direction of flow) is driven by diffusion. Solute concentrations can be modeled accurately, as laminar flow is predictable compared to the more chaotic turbulent flow of larger fluid reactors. The characteristics of microfluidic devices, small volumes, cellular-

scale dimensions, and laminar flow, are key advantages of these systems as physiologically relevant experimental platforms.

Though any given microfluidic device is still much cruder than a functioning organ, and still suffers from limitations of *in vitro* toxicity study, it is a large step forward from well-plate culture. Cell behavior in a microfluidic device is much closer to the behavior of a natural, functioning cell in the body. The microfluidic environment has been shown, for example, to include metabolic pathways in HepG2/C3As present in primary cell metabolism of acetaminophen *in vivo*, but absent in petri culture (Matthieu et al. 2011). HepG2 cell culture in microfluidic environment is well established (Leclerc et al. 2003). Design can be adjusted to address many limitations of well-plate culture. For instance, geometry can be controlled to mimic sinusoidal arrangement of *in vivo* cell conditions (Schutte et al. 2011). Other relevant cell types like intestinal or kidney cells can even be housed symbiotically with the hepatocytes (Sung, et al. 2010; Milwould et al. 2010).

Microfluidics is expanding rapidly as a platform for toxicity screening, but there is still much work to be done to make this a reliable, industry-ready method for pharmaceutical development. Complexity must be balanced with practicality for easy and widespread implementation in the lab. New methods for detecting metabolic activity are needed to noninvasively observe changes in metabolism due to drug exposure, for example using optical methods. Medium and cell fractions, staples of metabolic measurement in well-plate experimentation, are scarce or even inaccessible in a microfluidic reactor. Comprehensive analyses encompassing not only the immediate pathways of drug transformation but also many other relevant parts of intermediary

metabolism are needed to develop a more thorough and intricate understanding of the biochemistry underlying the hepatic response to drugs in order to interpret the measurements in a meaningful way.

Objectives

The long-term goal of this research is to elucidate the metabolic basis of idiosyncratic hepatoxicity, in particular toxic effects caused by drug-drug interaction. We focus on antidiabetic compounds because they are so widely prescribed, often in combinations with other drugs, and because diabetic patients are bodies under stresses that might exacerbate the effects of toxicity towards the liver. We assay a large number of metabolites in traditional well-plate experiments, including cofactors, which are central to cell metabolism and may provide early evidence of hepatic stress. We also develop a microfluidic platform for drug toxicity testing. This diffusion gradient chamber for the culture and drug treatment of HepG2 cells could, in the future, serve as an *in vitro* testing device for toxicity of a single drug, or drug interactions with other drugs or nutrients. This work also seeks to develop more intricate and sensitive methods for measuring metabolite concentrations to better detect early warning of stressful conditions on the hepatocytes.

Chapter 2: Materials and Methods

Materials and Reagents

HepG2 cells were obtained from ATCC (Manassas, VA). Dulbecco's modified Eagle medium (DMEM), fetal bovine serum (FBS), and penicillin-streptomycin were purchased from Invitrogen (Carlsbad, CA). Rat tail type 1 collagen was purchased from BD Biosciences (Bedford, MA). All other chemicals were purchased from Sigma (Saint Louis, MO) unless otherwise noted.

Cell Culture

HepG2 cells obtained as cryogenically frozen stock were expanded in T-75 flasks in high glucose DMEM with 10% FBS in an incubator at 37°C with 10% CO_2. Medium was replenished every other day until the cultures reached 80% confluence, at which point they were either sub-cultured or seeded into 12-well culture plates or microfluidic devices.

Microfluidics

Microfluidic Reactor

The microfluidic device consists of one central cell-culture chamber flanked by two medium channels. The medium channels and cell-culture chamber are separated by straight arrays of posts, which act as a permeable membrane and allow for diffusion across the cell culture region without any convective transport over the cells. The chip is accessible by six access ports located at the ends of the cell chamber and medium

channels. The chips were cast in polydimethylsiloxane (PDMS), a polymer that is soft, flexible, permeable to gasses, and optically transparent.

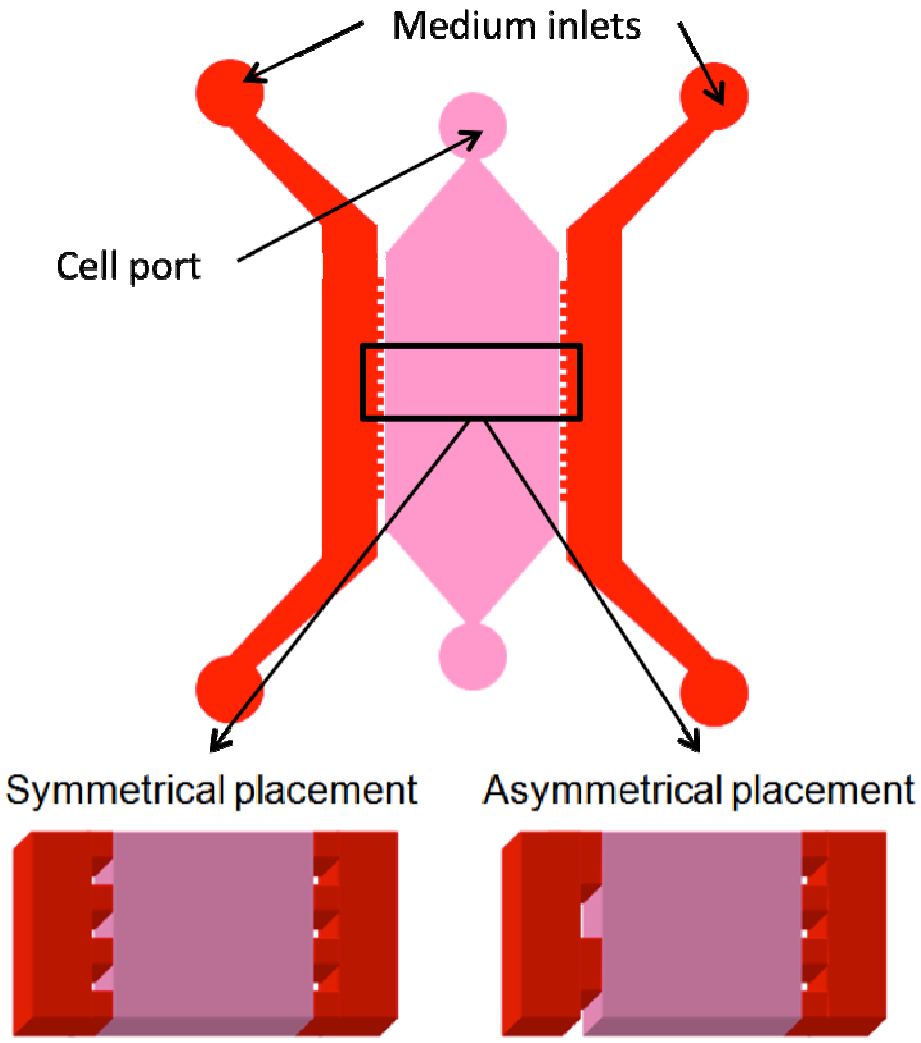

Figure 4: Schemiatic Representation of Microfluidic Reactor

Figure 4: Schematic representation of the micro-fluidic gradient culture device. The device consists of two distinct regions: a middle cell compartment and two flanking medium channels. A series of posts line the cell compartment and act as barriers against convective transport across the compartment. Post arrays are either symmetrical or asymmetrical for establishing linear and non-linear field gradients respectively.

A number of different device designs were evaluated. In the earliest designs the central cell culture chamber was very narrow, only 300 microns wide. The medium channels were 150 microns wide, the posts making up the membrane were 50 micron squares with 100 micron spacing, and all chip features were 100 microns in depth. This did allow for establishment of a drug gradient, but presented a few problems as well. Wide spacing of the posts allowed for cell migration out of the central chamber, and a small cell culture chamber limited the number of cells and the sensitivity of gradient we could attain in the reactor. In subsequent designs, the cell culture chamber was expanded laterally to a width of 1.8 mm allowing for more hepatocytes in the larger culture region. The post spacing was decreased to 20 µm to prevent cell migration from the central chamber.

Fabrication

Microfluidic reactors were fabricated using soft lithography and rapid prototyping (Whitesides et al. 2001). A high-resolution printer (20 µm feature size) (Page One, Irvine, CA) was used to create a transparency mask from a CAD file (Autodesk, San Rafael, CA). A 100 µm layer of SU8-50 photoresist (MicroChem, Newton, MA) was spin-coated onto a silicon wafer (Silicon, Inc., Boise, ID) to create a uniform layer of the appropriate height for chip features. The photoresist was exposed to light through the mask in a 1:1 feature ratio. Uncured photoresist was washed away, creating a negative master mold. PDMS (Sylgard 184, Dow Corning, Midland, MI) was then cast onto the master. Liquid monomer and initiator was poured onto the mold and kept under vacuum for several hours to eliminate bubbles. The PDMS was cured on a hotplate at 65 C overnight. The PDMS chips, now solid, were peeled from the silicon master (which could be reused many times). Individual chips were cut apart with a razor blade, taking care to

minimize exposure of the tiny chip features to dust and debris. Holes were punched with an 18-gauge blunt-end needle for fluidic interconnects taking care to remove the plugs between punches to guarantee unobstructed ports. The PDMS chips (still open and exposed) and glass slides were treated with oxygen plasma for 50 sec (Plasma cleaner Model PDC-001, Harrick Plasma, Ithaca, NY). The chips were then carefully assembled by sealing to the glass slides and bonded at 125°C overnight.

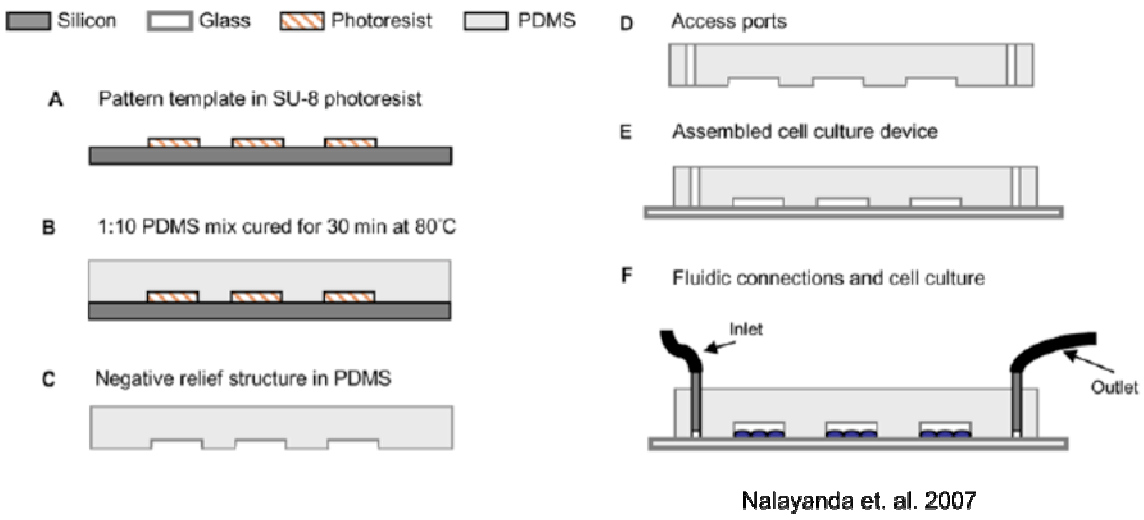

Figure 5: Fabrication of Master Mold and PDMS Chip

Figure 5: Fabrication of silicon/photoresist master and PDMS chips from Nalayanda et al. 2007

Modeling

Simulations were performed using the Multiphysics® software (COMSOL, Burlington, MA). Medium flow rates and post sizes were varied to identify reactor dimensions and operating conditions that support cell growth and maintenance.

Collagen Gel: $$\frac{\partial c}{\partial t} = (\nabla \cdot D_\alpha \nabla c) - u \cdot \nabla c$$

Gel Phase (β): $$\frac{\partial c_\beta}{\partial t} = \nabla \cdot D_\beta \nabla c_\beta - r$$

Cell Phase (γ): $$\frac{\partial c_\gamma}{\partial t} = \nabla \cdot D_\gamma \nabla c_\gamma - r$$

Nutrient Consumption Rate: $$r = \frac{Q_m \cdot c_\gamma}{K_m + c_\gamma}$$

Monod Kinetics :

(O_2 availability limits overall growth rate) $$\mu = \frac{\mu_{\max} \cdot c}{K_s + c}$$

Boundary conditions:

Microfluidic Feature Edges

Insulation/Symmetry

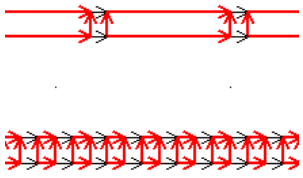

$$\boldsymbol{n} \cdot \boldsymbol{N} = 0$$

$$\boldsymbol{N} = -D\nabla c + c\boldsymbol{u}$$

Spaces between Posts

Continuity

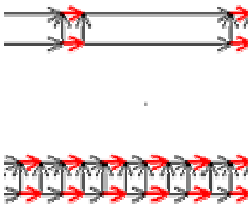

$$N_i = -D_1 \nabla c_i + c_i u_i$$

$$n \cdot (N_1 - N_2) = 0$$

Medium Inlet

Concentration

$$c = c_0$$

Medium Outlet

Convective flux

$$n \cdot (-D \nabla c) = 0$$

c: limiting nutrient (i.e. O_2) concentration

D: diffusion coefficient; subscript denotes phase

μ_{max}: max hepatocyte specific growth rate

K_m: oxygen affinity constant

K_S: Monod constant (=K_m)

Q_m: hepatocyte max oxygen uptake rate (OUR)

K_{eq}: equilibrium partition constant for O_2

Cell Culture in Microfluidic Reactor

The middle culture chamber of the microfluidic device was pre-coated with a dilute solution of type I collagen in PBS (0.36 mg/mL) and incubated for 1 hr at room temperature. HepG2 cells were seeded using a cell suspension of ~6 million cells/mL.

To reduce clumping, high concentrations of TE Express were used when passing the cells from T-flask to the microfluidic device (50% TE, 50% growth medium at seeding) and cells were agitated vigorously many times before they were introduced into the microfluidic chamber. The seeding medium was replaced with growth medium after a few hours (~ 2 hrs) when a majority of the cells had settled onto the collagen-coated slide. A small droplet of the growth medium was added to one cell injection port to establish a gravity-driven flow through the chamber, displacing the seeding solution without detaching the weakly adherent cells.

Once the cells adhered (~4 hrs), the medium channels were also filled with the growth medium, again by adding small droplets to the ports. All ports were topped with large droplets of medium, and the entire device was placed in a Petri dish containing sterile water. Care was taken not to top the device with the water. The wet Petri dish acted as a humidity chamber, preventing loss of medium from the ports due to evaporation. The entire assembly was then placed in a humidified incubator (37 °C, 10% CO_2) overnight.

After overnight incubation, each inlet of the medium channels was connected with 1.09-mm OD polyethylene (PET) tubing to a constant flow syringe filled with pre-warmed growth medium. The constant flow syringe consists of two nested containers. Medium drips from the inner container to the outer container through a side port, resulting in a nearly constant flow rate from the bottom of the outer container. Average flow velocities in the medium channels were estimated to be approximately 3~4 μL/min based on the volume discharged. Uniform elevation and head pressures maintained the same flow rate for both medium channels. The medium channel outlets were connected

with PET tubing to a waste reservoir at a lower elevation. Care was taken when connecting the tubing to ensure that flow is unobstructed by debris, bubbles, or other impediment (e.g. pinched tubing or tubing pressed flush to the glass slide). The microfluidic device, tubing, syringes and waste reservoir were placed in an incubator to maintain control over temperature and medium pH. Drug treatments began on day 3 after cell seeding, when the culture reached confluence.

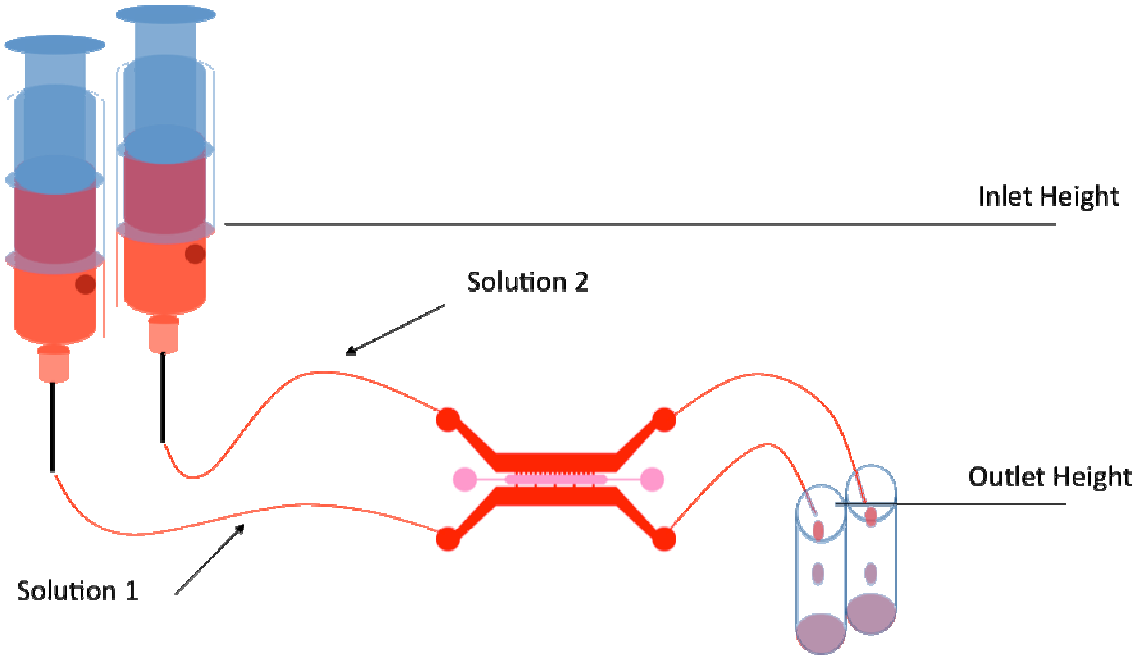

Figure 6: Cell Culture in Microfluidic Reactor

Figure 6: Gravity driven flow from constant-flow syringes, through medium channels, and out to a waste collection beaker.

Effects of Troglitazone on HepG2 Cells in Microfluidic Reactor

Troglitazone (TGZ) was used to demonstrate that a toxicity gradient could be established within the microfluidic culture device. On day 3, cells were observed with Live-Dead staining to establish a baseline prior to drug exposure (1.6 µM calcein and 1.6 µm ethidium homodimer-1 in both medium channels). A steep gradient of TGZ (0.5 mM

TGZ at the source channel and no drug at the sink channel) was then established across the cells. After 24 hours, the cells were observed with Live-Dead staining once more. The gradient experiment was repeated using lower levels of TGZ (0.01 mM at the source and no drug at the sink) and glucose background (1.0 g/L) for a longer time period of 4 days. In separate experiments, we expose the cells to a gradient in the glucose level (4.5 g/L at the source and 1.0 g/L at the sink) while holding constant the level of TGZ (0.05 mM in both medium channels) to determine whether the medium glucose level affects the toxicity of TGZ.

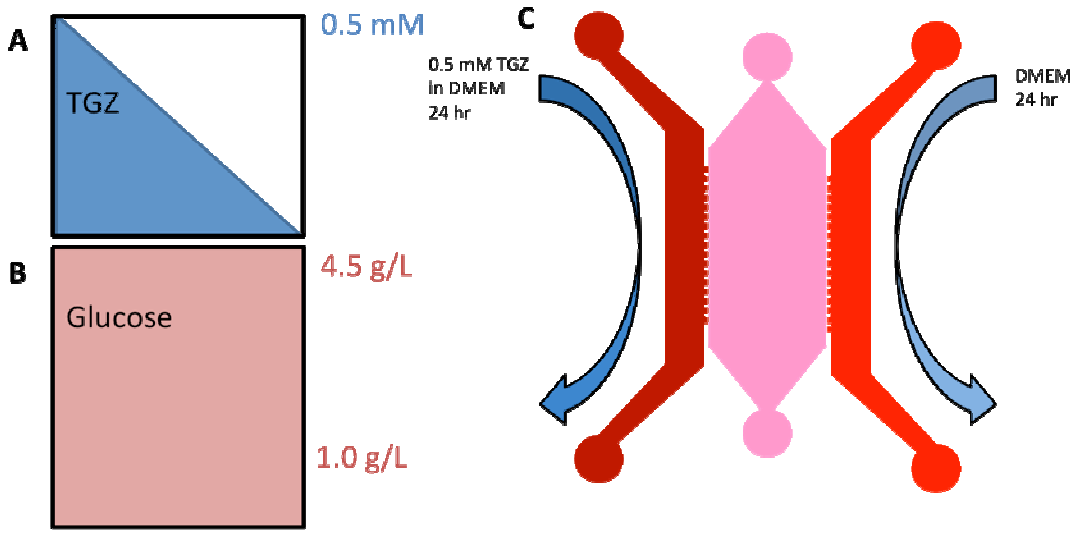

Figure 7: Microfluidic Experiment TGZ Gradient

Figure 7: (A) A concentrated gradient of TGZ was applied in a uniform environment of high glucose DMEM (B). (C) The cells were exposed to this gradient of 0.5 mM TGZ at the source and 0 at the sink for 24 hours.

Well Plate Experiments

HepG2 cells previously expanded in a T-75 flask were seeded into 12-well plates at a density of 1.8×10^5 cells per well. The seeding volume was 1 mL. The well plates were placed in an incubator at 10% CO_2 and 37 C for several hours to allow the cells to settle and attach to the tissue culture plate. After cell attachment, 500 µL of medium was removed from each well, leaving a final culture volume of 500 µL per well. We found that seeding the cells using a higher volume of medium (relative to the final culture volume) more evenly distributed the cells over the culture surface. When seeded using the final culture volume, the center of the well was only sparsely populated with cells relative to the outer rim of well. Over time, the cells in the rim form an overgrown ring, while the cells near the center never reaches confluence. Uniformly seeded cultures were grown for 10 days, during which time the culture medium was replenished every 2 days. All drug exposure experiments were started on day 10 of well-plate culture.

TGZ Experiments

Cells in 12-well plates were initially exposed to 0, 50, or 100 µM TGZ in high glucose DMEM supplemented with 10 % FBS. In a subsequent experiment, the drug doses were reduced (up to 25 µM) to examine the metabolic effects at sub-toxic doses (Yamamoto et al. 2002). The drug was added to the culture medium dissolved in ethanol. The untreated control received only the solvent. The final solvent concentration in both the treated and untreated conditions was 0.25 % (v/v). Medium and cell samples were collected at 4, 8, 12, 24, 36, and 48 hours. The spent medium samples were cleaned of cell debris by a brief centrifugation step. Cells were lysed *in situ* with a 0.1% SDS buffer and sonicated. The samples were stored frozen at -20 C until further analysis.

Metabolite and DNA measurements were performed on spent medium samples and cell lysates, respectively.

Metformin and Rosiglitazone Drug Interaction Experiments

HepG2 cells were cultured in 12-well plates as previously described. On day 10 of culture, the cells were treated with the following combinations of drugs and doses (Table 1):

Table 1: Treatment Conditions for Metformin and RGZ Exposure

Condition	**Abbreviation**	**Concentration Metformin (µM)**	**Concentration ROSI (µM)**
Control	0	0	0
Low Dose Metformin	ML	500	0
High Dose Metformin	MH	2000	0
Low Dose ROSI	RL	0	5
High Dose ROSI	RH	0	10
Both Drugs, Low Dose	BL	500	5
Both Drugs, High Dose	BH	2000	10

At 24 and 48 hours, spent medium and lysed cell samples were collected, cleaned, and stored as previously described.

Analytical Methods

Medium samples were analyzed for amino acid content using HPLC and drug content using liquid chromatography-mass spectrometry (LC-MS). Glucose and lactate concentrations were measured using enzymatic assays according to the methods of Trinder (1969) and Loomis (1961), respectively. Lysed cell fractions were analyzed for DNA content and cofactor metabolites using the Hoechst dye and LC-MS, respectively. All metabolite data were normalized by the corresponding cell sample DNA content.

Amino Acid Analysis

Glucose and lactate concentrations were measured using the methods of Trinder (Trinder, 1969) and Loomis (Loomis, 1961), respectively. Amino acids were quantified by HPLC (Alliance 2690, Waters, Milford, MA) using fluorescence-based detection following pre-column derivatization of primary or secondary amines with 6-aminoquinolyl-N-hydroxysuccinimidyl-carbamate (Cohen and De Antonis, 1994).

DNA Assay

DNA concentration was determined using the Hoechst dye method (Si et al. 2004). Cell samples were diluted {what-fold?} to bring the DNA content in the samples into the linear range of detection. A standard curve was generated from a stock solution (50 µg/mL) of calf thymus DNA (Sigma). Twenty µL of each standard or sample was added to a well with 200 µL of Hoechst dye solution. The plates were incubated at room temperature for 20 minutes before measuring fluorescence at excitation/emission of 365/458 nm.

Lactate Assay

Lactic acid concentration was determined with a commercial lactate standard set and lactate assay reagent (Trinity Biotechnology). Samples were diluted 5-fold to put them in the linear range of the assay. In each well of the assay plate, 10 µL diluted sample and 200 µL working reagent was added. The plates were incubated at 37 C for 5 minutes, and absorbance was measured at 540 nm.

Glucose Assay

Glucose concentration was determined with glucose oxidase reagent (Pointe Scientific INC) and standards of D-(+)-Glucose (Sigma). Glucose standards of 0, 1, 2, and 3 g/L were prepared by serial dilution. Glucose oxidase reagent was reconstituted according to manufacturer's instructions and pre-incubated at 37 C immediately before use in the assay. Medium samples were diluted two-fold with deionized water. Into the wells of a 96-well assay plate were added 5 µL diluted sample and 300µL glucose oxidase reagent. The plates were then incubated at 37 C for 30 minutes and the absorbance was measured at 500 nm.

Liquid Chromatography-Mass Spectrometry (LC-MS)

All LC-MS studies were run on an Applied Biosystems 3200 QTRAP mass spectrometer (acquired by Life Technologies, Carlsbad, CA) with a 1200 series binary pump and autosampler from Agilent Technologies (Santa Clara, CA). Data was analyzed on Analyst software 1.5.1 with mass spec toolkit version 3.3 (Sierra Analytical, Laguna Hills, CA).

TGZ Detection by LC-MS

TGZ standards and medium samples were prepared by mixing 30 µL of sample with 90 µL ice cold acetonitrile. The samples were centrifuged at 10,000 rpm for 5 minutes, and

the supernatant collected for analysis. TGZ concentrations were quantified using liquid chromatography-mass spectrometry (LC-MS). The analysis was performed on a 3200 QTRAP Hybrid Triple Quadrupole Linear Ion Trap mass spectrometer (AB SCIEX, Foster City, CA) coupled to a 1200 Series Binary LC System (Agilent Technologies, Santa Clara, CA). Chromatographic separation used a Synergi Fusion-RP polar embedded C18 column (Phenomenex, Torrance, CA). The mobile phase composition was ramped linearly from 10% acetonitrile and 90% water to 80% acetonitrile and 20% water at 35 min. The mass spectrometer was operated in positive ion mode with multiple reaction monitoring (MRM) for parent/fragment ion pair with m/z 422.2/165.2. The TGZ peak was observed at 34 min, and quantified based on peak area comparisons to the standards using Analyst software version 1.5 (AB SCIEX).

(as described in Kassahun et al. 2001). Samples were analyzed for TGZ, and also for all TGZ derivatives described by Kassahun et al.

Metformin and Rosiglitazone Detection by LC-MS

Cofactors were separated with a gradient of the following solvents, A: water with 0.1% formic acid and solvent B: acetonitrile. The method ramped linearly from 100% solvent A (aqueous phase), to 10% A and 90% B by 20 minutes with a 5 minute linear recovery. Pressure was 400 µL/min in all cases. Metformin was detected around 2 minutes, and ROSI closer to 10 minutes.

Detection of Energy Cofactors by LC-MS

To separate cofactors ADP, ATP, NAD, NADH, NADP, and NADPH, we used a Synergi Fusion-RP polar embedded C18 column (Phenomenex, Torrance, CA) and the following solvents: (A) 0.015 M Tributyl amine with 0.01 M acetic acid and (B)

methanol. Separation was obtained using a gradient-based LC method with the elution profile shown in Table 2. The MS was run in negative ion mode with an ion spray voltage of 4500 {unit?}. Multiple reaction monitoring (MRM) was used to detect each of the cofactors.

Table 2: Solvent profile for separating cofactors: NAD, NADH, NADP, NADPH, ATP, ADP.

Time (min)	Flow (µL/min)	%A	%B
0	200	80	20
5	200	80	20
10	200	68	32
15	200	65	35
20	200	40	60
25	200	10	90
35	200	10	90
35.1	200	20	80
43	200	20	80

All transitions are linear. See text for solvent A and B compositions.

TGZ Drug Derivatives

Following the protocols outlined by Kassahun et al. in their comprehensive detection of TGZ reactive intermediates by MRM, we sought to detect for the following conjugates (labeled M1 through M5) in our samples:

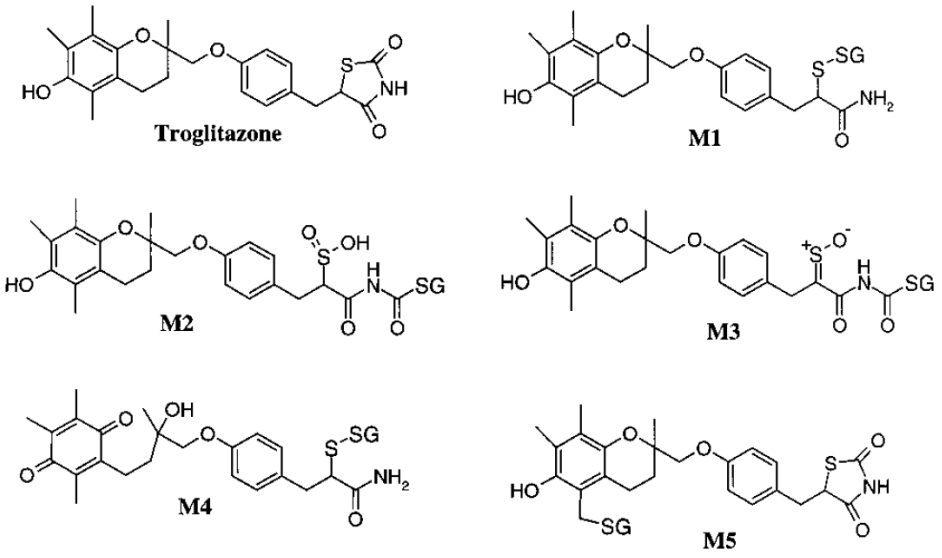

Figure 8: TGZ and Its Reactive Intermediates

Figure 8: Troglitazone and five of its reactive intermediates (M1-M5) which may play a role in the drug's idiosyncratic hepatoxicity (Kassahun et al 2000)

Chapter 3: Microfluidic Reactor Results

Establishment of Cell Culture

After some experimentation, reliable cell culture was attained in the microfluidic devices. Coating the central cell chamber with collagen significantly aided cell adherence to the surface. Seeding at a high cell density was vital to achieve uniform coverage necessary for experiments; however to attain this high seeding density, the tendency of HepG2s to clump together had to be overcome. The high levels of TE express used in detaching the cells helped, as did persistent vigorous pipetting to break up the cell clumps. Though there was some concern that viability may be compromised due to the protease treatment and the shear stress induced by pipetting, subsequent growth of the HepG2 cells was unaffected. Sparse seeding at a lower cell density led to patchy coverage, while clumpy seeding led to overgrown areas in the culture chamber that limited diffusion across the cell chamber (data not shown). In contrast, uniform coverage at confluence was achieved by seeding at high cell density using the protease treatment and additional pipetting steps (Figures 10 and 11).

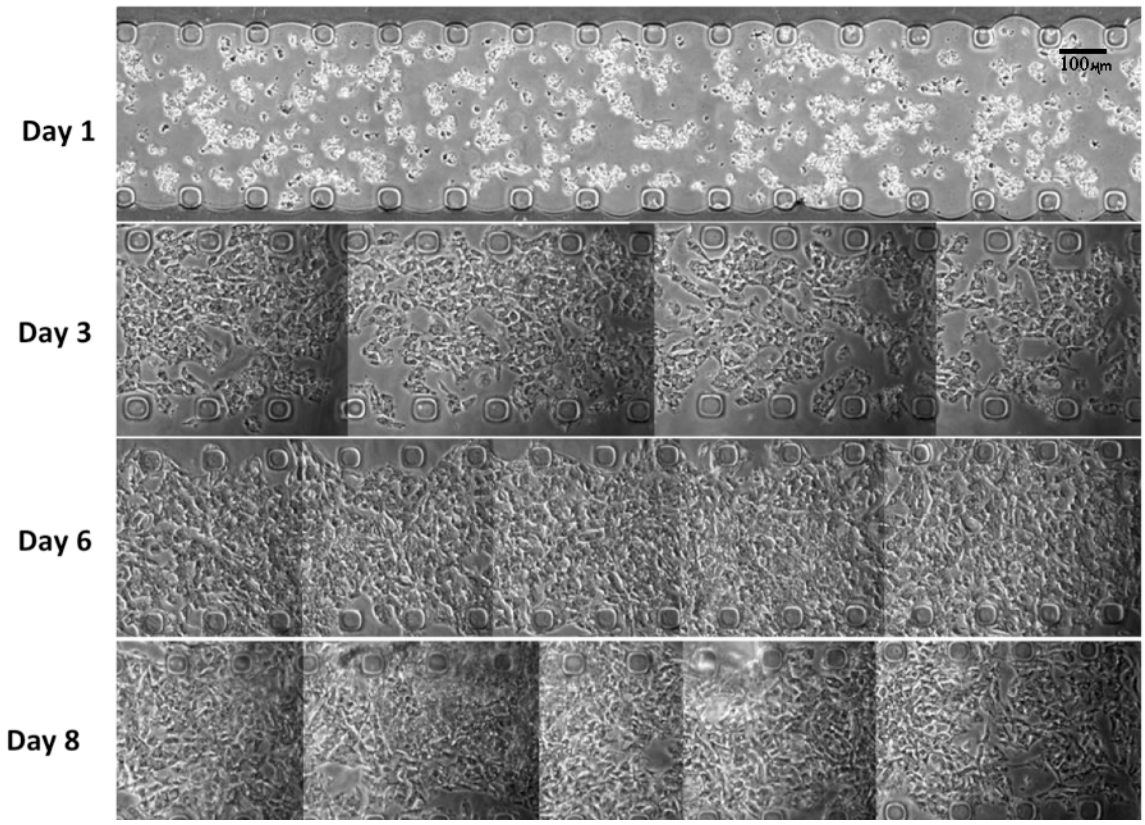

Figure 9: Cell Proliferation in Microfluidic Reactor

Figure 9: Phase contrast images of cell proliferation during the first week of reactor culture in early reactors (posts, 50 x 50 μm spaced 100 μm apart, culture chamber 300 μm wide). Cells were loaded into the culture chamber on day 1. Medium flow was driven by setting up a constant gravitational potential difference across the inlet and outlet ports. The flow rate in the channels was maintained at 4 μL/min throughout the culture period. Culture device and gravity-driven flow assembly were kept at 37 °C inside a cell culture incubator with humidified air and 10% CO_2.

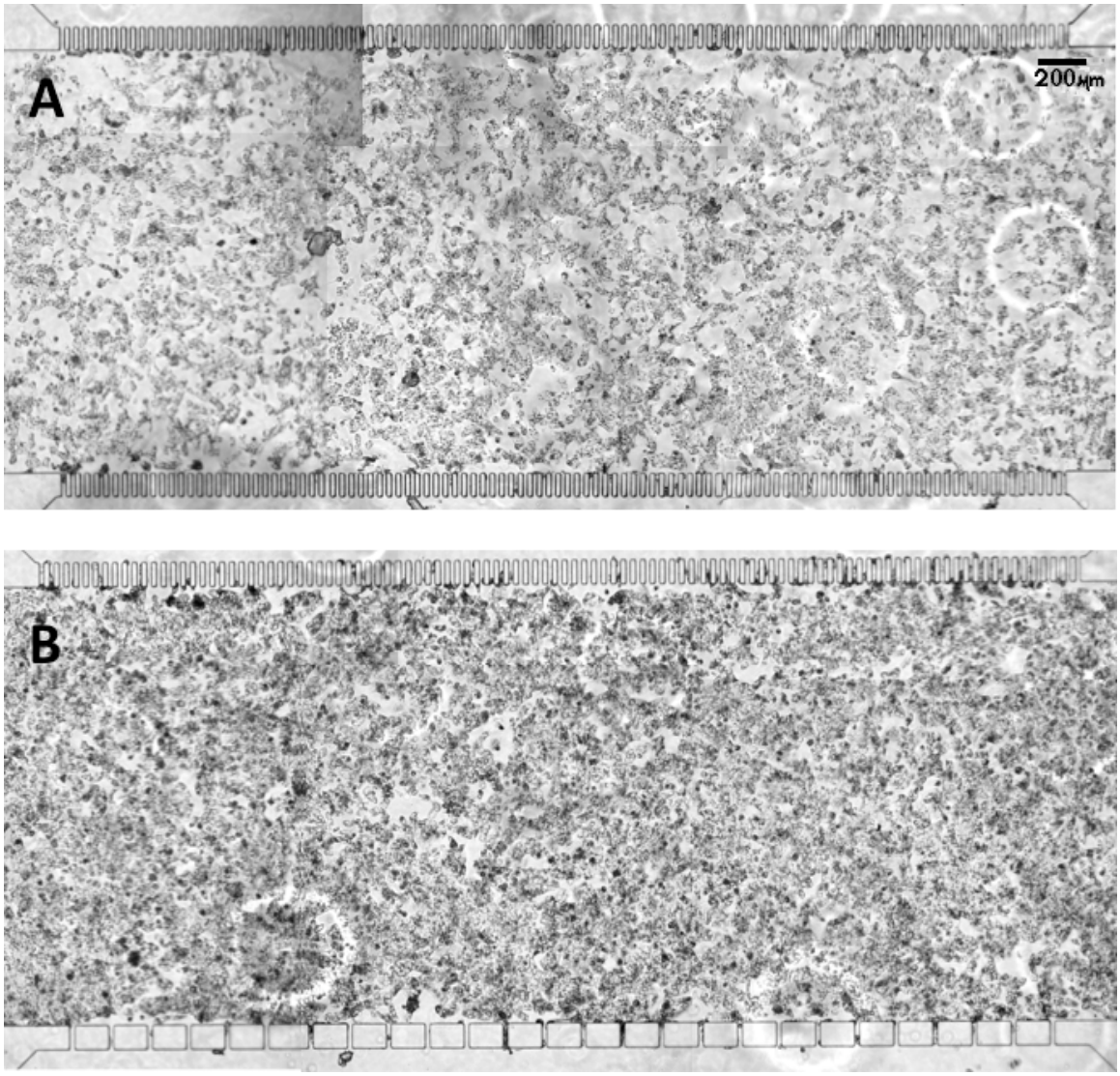

Figure 10: Microfluidic Reactor Images

Figure 10: Phase contrast images of HepG2 cells in cell culture chamber with (A) symmetrical and (B) asymmetrical post arrays on day 3 of cell culture. The cell culture chamber is 1.8 mm across with 20 μm post spacing.

Establishment of a Steady State Diffusion Gradient

To establish a diffusion gradient across the cell culture region, one constant flow syringe was filled with solute-spiked medium. As the medium flowed through the medium channels, the solute diffused through the post array and across the cell culture

region towards the unspiked medium channel on the opposite side. In a preliminary study, we examined diffusion of Allura food coloring (1.25µg/ml at the source, 0 at the sink). In agreement with the model, a steady state gradient was established across a collagen gel-filled cell chamber within 3 hours.

To demonstrate that a diffusion gradient could be established across a culture chamber seeded with HepG2 cells, a gradient of a fluorescent cell stain (calcein) was applied across the culture (1.2 µM at the source, 0 at the sink). As expected, the calcein dye only stained a region of cells near the source channel, even though the culture chamber was uniformly covered with cells (Figure 11).

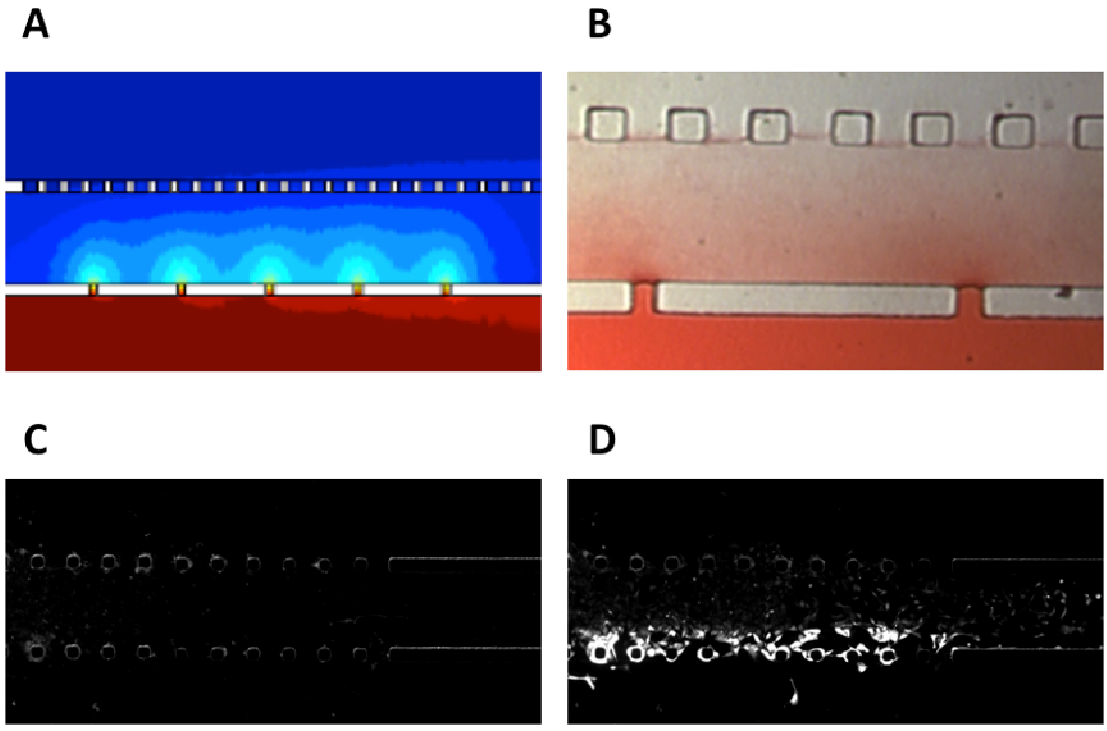

Figure 11: Establishmeint of Steady State Diffusion Gradient in Microfluidic Reactor

Figure 11: (A) Predicted diffusion gradient across the cell compartment in an asymmetrical chip (early design). The solute diffuses from the bottom (source) to the top (sink). (B) A concentration field of the food coloring dye Allura (1.25 μg/ml) (Sigma, St. Louis, MO). A steady field gradient was established in ca. 3 hrs, in good agreement with the model prediction. Courtesy of Ning Lai (C) Dead cells dyed with EthD-1 are sparse and uniformly distributed across the cell chamber. (D) Live cells dyed with a gradient of calcein from 1.2 μM at source to 0 at sink.

After this proof of principle, the cells were exposed to a gradient of very high dosage of TGZ to demonstrate a gradient-dependent toxic effect on HepG2 cells. The cells showed clear toxicity in correspondence with their drug dosage. All cells on the source channel (0.5 mM TGZ) side of the reactor were dead, while the cells exposed to a lower dosage near the sink channel remained viable. Though the Live/Dead assay is a rather crude measure of toxicity, this experiment showed that the microfluidic culture device could be used to determine the effects of a drug gradient on HepG2 cells.

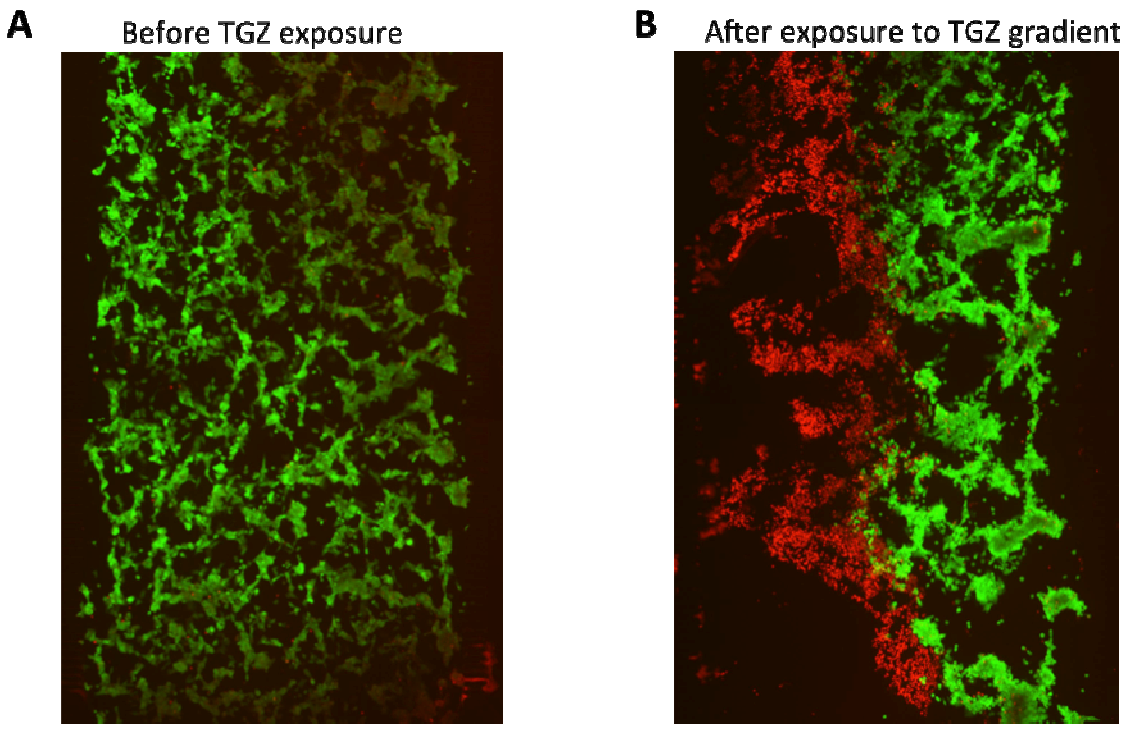

Figure 12: Toxic Effects of Steady State Drug Gradient

Figure 12: (A) Cells are healthy and living (green) on day 3 of cell culture in the microfluidic reactor. Dead cells (red) are few and evenly dispersed in the reactor. (B) After exposure to a gradient of TGZ (0.5 mM at source, 0 at sink), the hepatocytes exposed to a high concentration (left side of reactor) are all dead. Cells on the right, exposed to lower doses of TGZ, are still living.

In Figure 12, there is a clear transition between Live and Dead staining. Image processing was used to analyze the data more quantitatively. A series of line-cuts were made across the cell chamber using Image J software. The light intensity for each dye was summed and then normalized. For each physical position, x (as measured from the source side of the cell culture region), the normalized brightness was graphed for both live and dead marker dyes. There is a clear shift in the center of the reactor, around 0.9

mm. Model calculations showed the transition occurred at a concentration of TGZ around 0.25 mM.

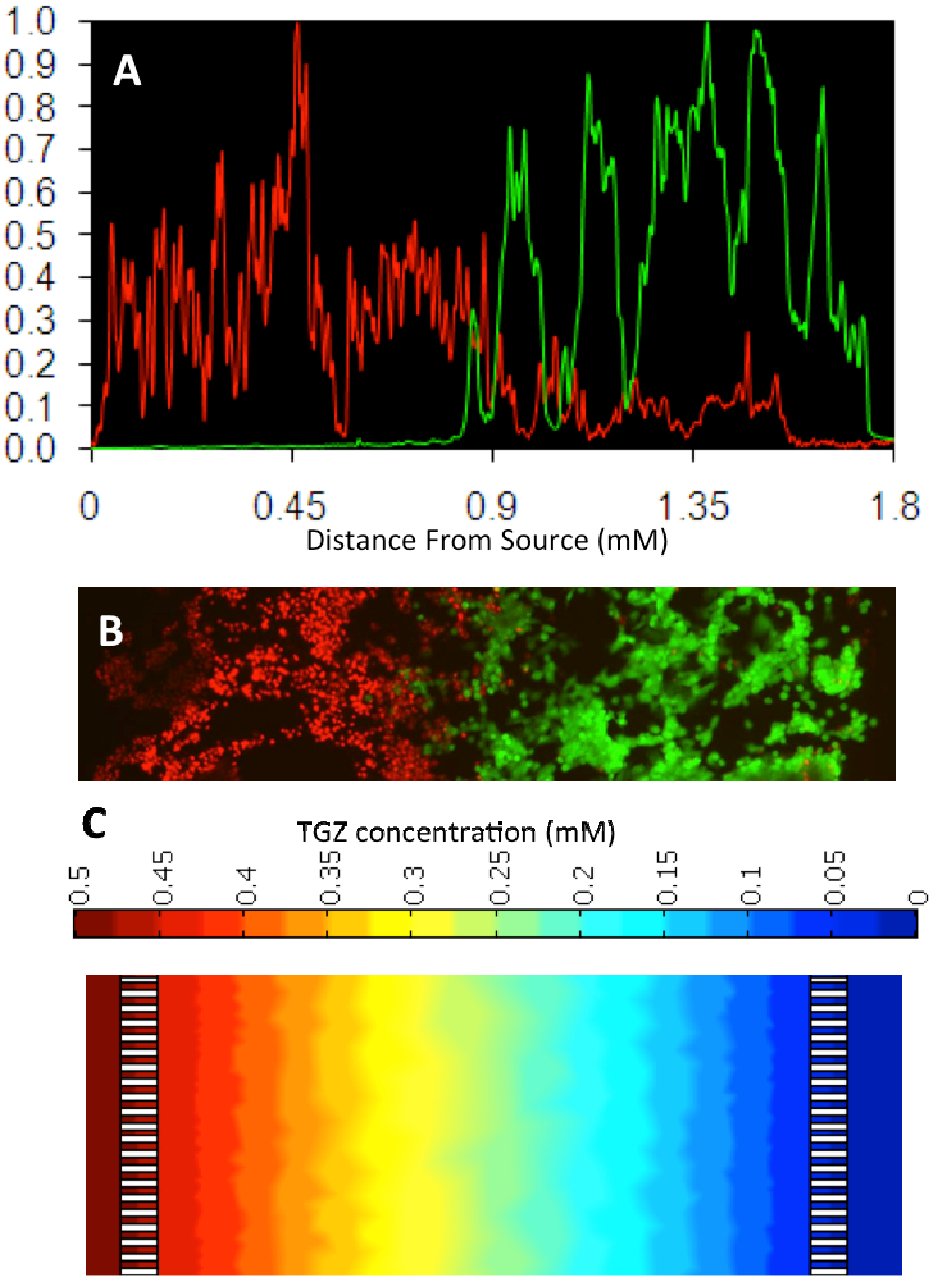

Figure 13: Image Processing and Modeling for Drug Gradient in Microfluidic Reactor

Figure 13: (A) Normalized intensity of line cuts across (B) a section of the cell-culture chamber indicate a transition from dead to live cells at approximately the center of the chamber, 0.9 mm. (C) The model indicates that for this linear gradient, 0.9 mm corresponds to a TGZ concentration of 0.25 mM.

The drug gradient experiment was repeated using a lower, sub-toxic level of TGZ (0.01 mM in the source channel) and a physiological level of glucose (1.0 g/L in both medium channels). At these levels, the Live-Dead staining technique did not show a significant effect of the drug gradient. Although there does appear to be some increased toxicity on the source side, the effect is small and not statistically significant.

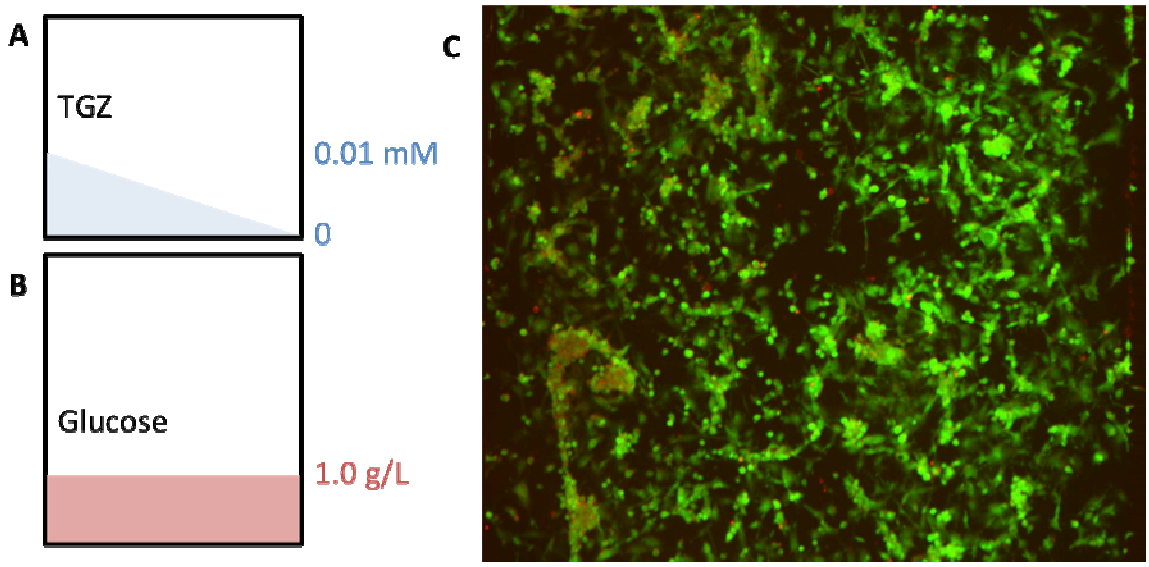

Figure 14: Establishment of Low-Dose TGZ Gradient in Microfluidic Reactor

Figure 14: A less concentrated gradient of TGZ (A) was applied against a background of uniformly low glucose in the culture medium (B). Under these conditions, the Live-Dead stain showed no measureable gradient of toxicity. A more sensitive probe is needed to gain more detailed information about the effects of the drug.

Examining TGZ/Nutrient Interactions

To examine the effect of the nutrient background, we conducted a gradient exposure experiment with a constant low dose of TGZ (0.05 mM in both medium channels) and a gradient of glucose (4.5 g/L glucose in source channel and 1.0 g/L glucose in sink channel). The cells on the source (high glucose) side of the gradient showed greater cell death after 4 days of exposure to the drug compared the cells on the sink (low glucose) side. This is interesting to note, because a diabetic person (who would be prescribed a drug like TGZ) will exhibit chronically elevated blood glucose levels.

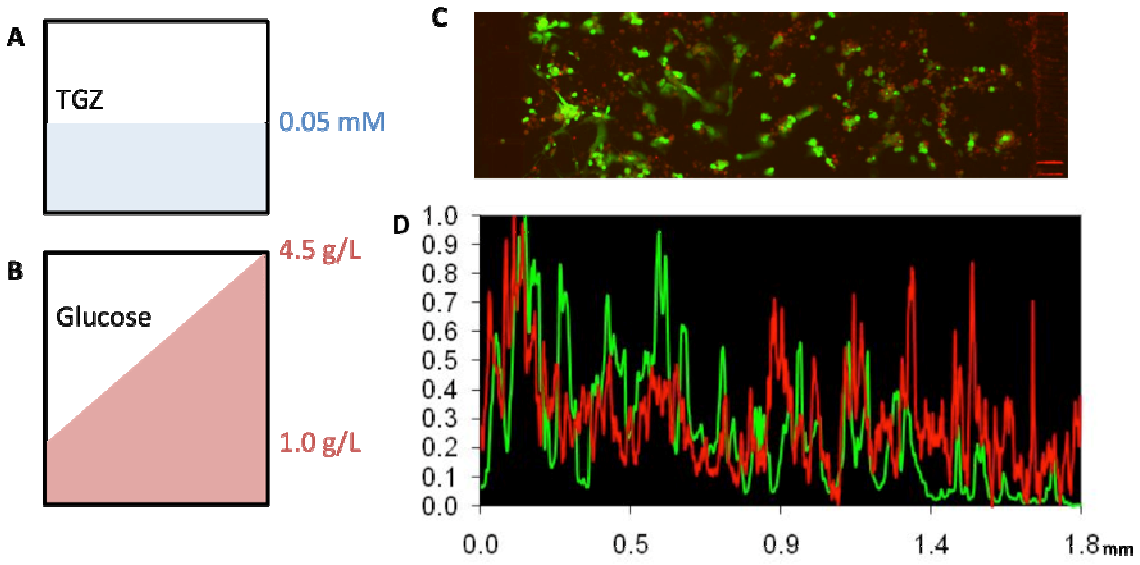

Figure 15: Establishment of Glucose Gradient in Presence of TGZ

Figure 15: (A) A low dose of trogiltazone was applied to the whole reactor with (B) a gradient of glucose in DMEM (1.0 g/L glucose at left, 4.5 g/L glucose at right). (C) After four days of this steady state drug/glucose gradient, live dead staining shows slightly more cell death on the high-glucose side of the reactor. (D) This relationship is supported by image processing analysis.

Discussion

A microfludic reactor was developed for the culture of HepG2 cells and the establishment of steady state diffusion gradients across the cell culture region. Because these reactors are designed on the micro-scale, transport is dominated by diffusion, and is very predictable. HepG2 cells can be cultured in these reactors on the order of weeks. Steady state diffusion gradients were established in accordance with model predictions. These models allow for accurate information about the chemical environment of a cell at any position in the reactor. Live-dead staining was used as an optical indicator of cell death to illustrate how one might assess cell stress at different concentrations within the reactor. Though a crude measure of metabolic burden, the live-dead staining did show clear cell death at extremely high doses, and also increased cell death when low levels of TGZ were applied under high glucose conditions. This microfluidic reactor for cell culture and diffusion gradient can be used with any optical indicator of cellular metabolism to assess, in one experiment, many different conditions of drug dosage or interaction. Such a platform could prove very useful in the development of safe drugs and understanding of drug interactions with other drugs or nutrients.

Chapter 4: Results of Metabolic Studies of Troglitazone on HepG2 Cells in Well-Plate Culture

High Concentration of TGZ

Released in 1997, TGZ had to be pulled from the market in 2000 due to multiple instances of adverse and idiosyncratic liver failure. TGZ was chosen as a drug candidate for our trials because it is a known toxic risk for unknown reason. To try to explain its toxicity, we sought reactive intermediates in all of our samples, but were unable to reproduce detection of TGZ conjugates demonstrated by Kassahun, 2002.

To reproduce some of the toxic effects of TGZ in our well plate studies, we started with very high dosages of the drug. At doses of 0.05 and 0.1 mM, TGZ leads to significant loss in cell viability (Figure 16). Interestingly, there was a net loss of cells at 48 hours for all treatment conditions, presumably due to an exhaustion of nutrients and/or accumulation of harmful waste metabolites. To characterize in more detail the effects on cellular metabolism, we also analyzed the production and consumption of amino acids. Measurements on medium samples showed significant differences in the levels of several amino acids (Figure 17).

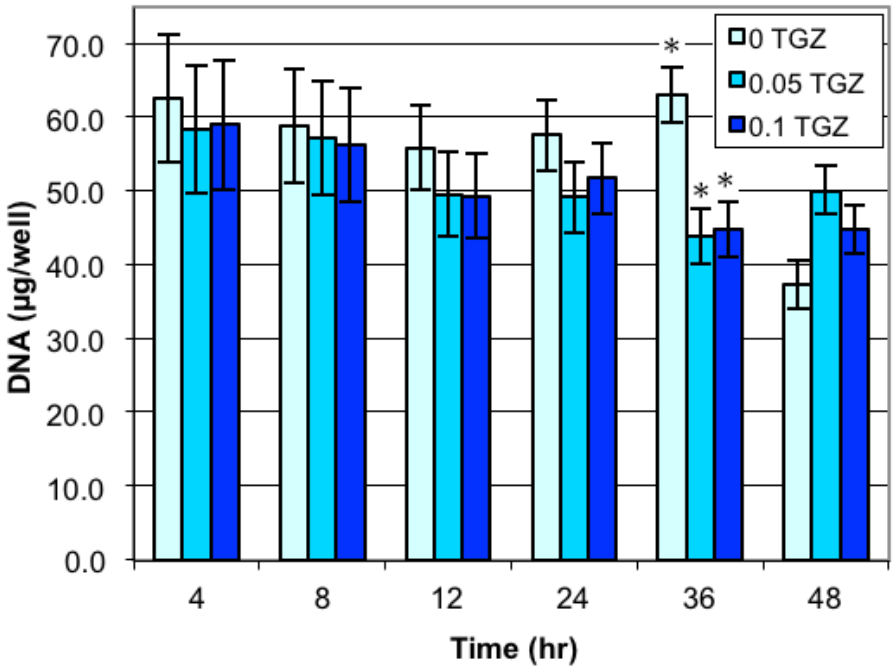

Figure 16: DNA Data After Treatment With TGZ

Figure 16: Effect of TGZ treatment on culture DNA. Drug doses measured in mM. *: Statistically significantly different from control at $p < 0.05$.

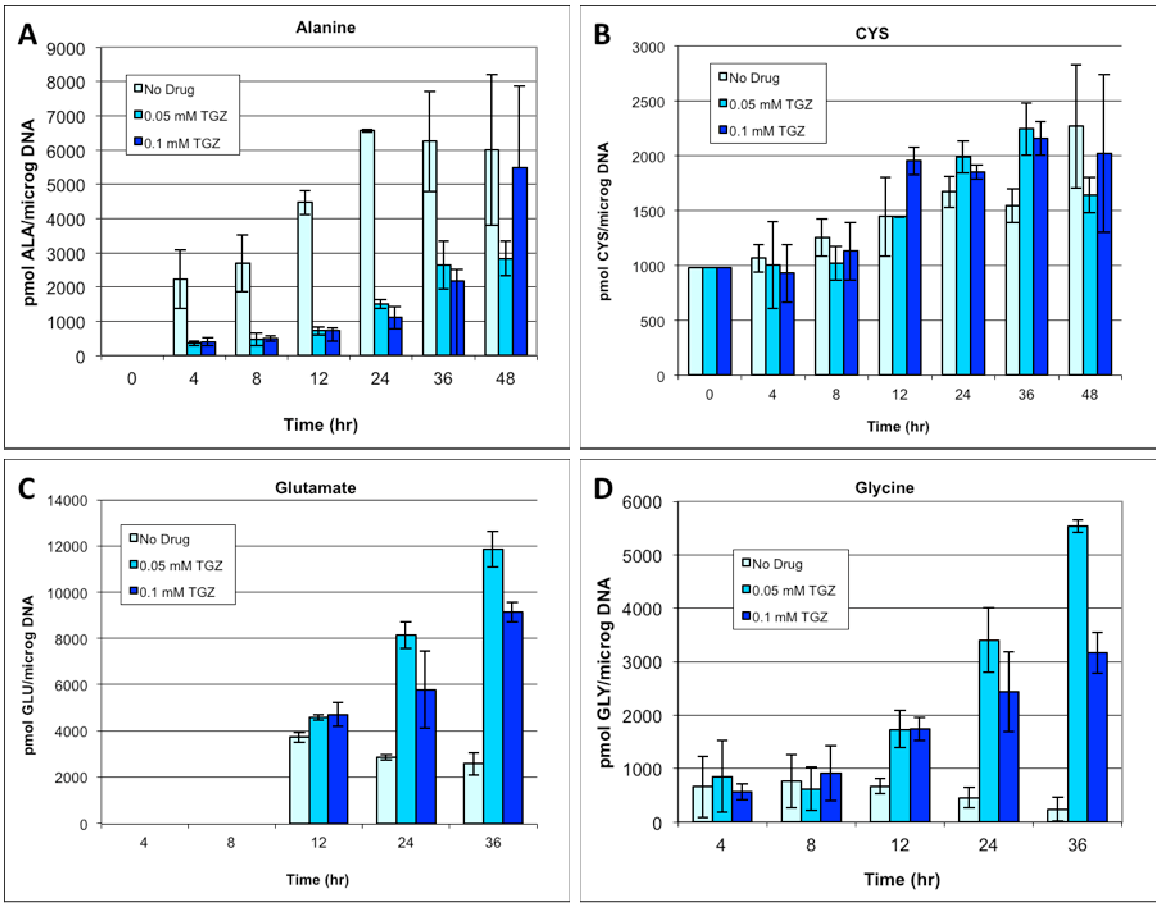

Figure 17: Amino Acid Data After TGZ Treatment

Figure 17: Effect of TGZ treatment on amino acid production and consumption. (A) Treatment with TGZ suppresses alanine production in HepG2. (B) Cystine shows no substantial differences, which is curious as cystine is one of the few amino acids with a sulfur group, and one might expect that to interact with the TGZ molecule. TGZ increases production of both glutamate (C) and glycine (D) as compared to control. Error bars are standard deviations of the mean from triple replicate of each experimental condition.

Physiologically Relevant Doses of TGZ

As was the case for the microfluidic device experiments, the lower concentrations of TGZ did not significantly affect the culture viability as assessed by DNA measurements.

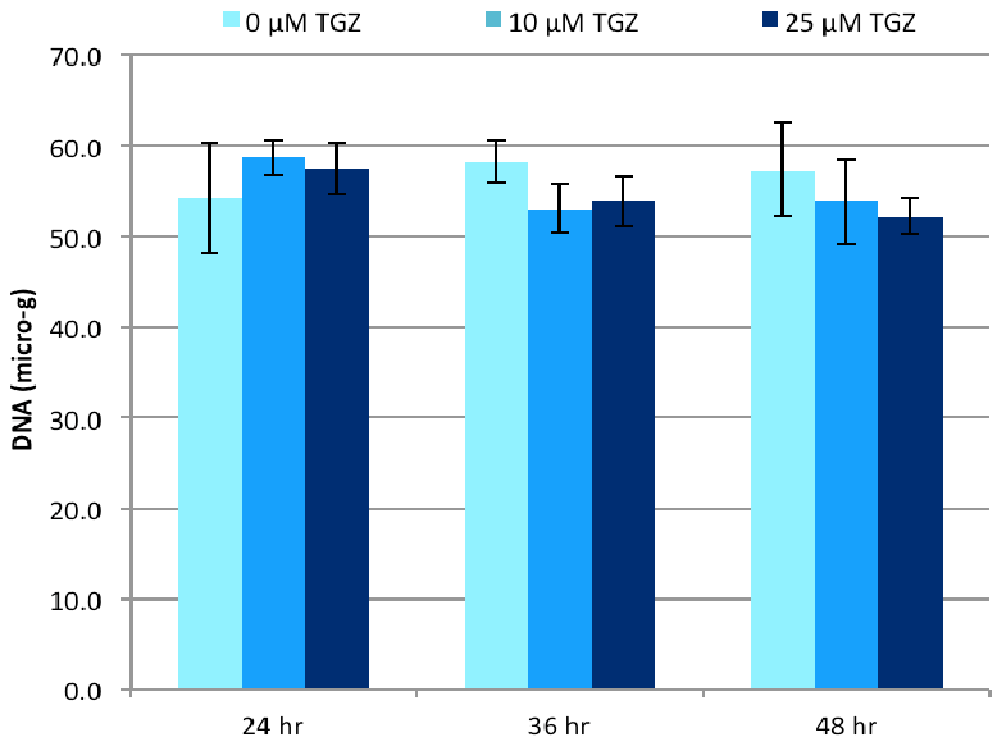

Figure 18: DNA Data After Treatment With Low Dose of TGZ

Figure 18: Effect of low dose TGZ treatment on culture viability. While there was a small decrease in culture DNA over time with the drug treatments, the decrease was not significant.

Similarly, statistically significant differences were not observed for amino acid levels in the culture medium (data not shown).

TGZ Consumption

TGZ was easily detectable with LC-MS. The level of TGZ remains constant for the first 24 hours, and then drops off rapidly. For both 10 and 25 μM doses, the drug is completely metabolized by the cells at 48 hours.

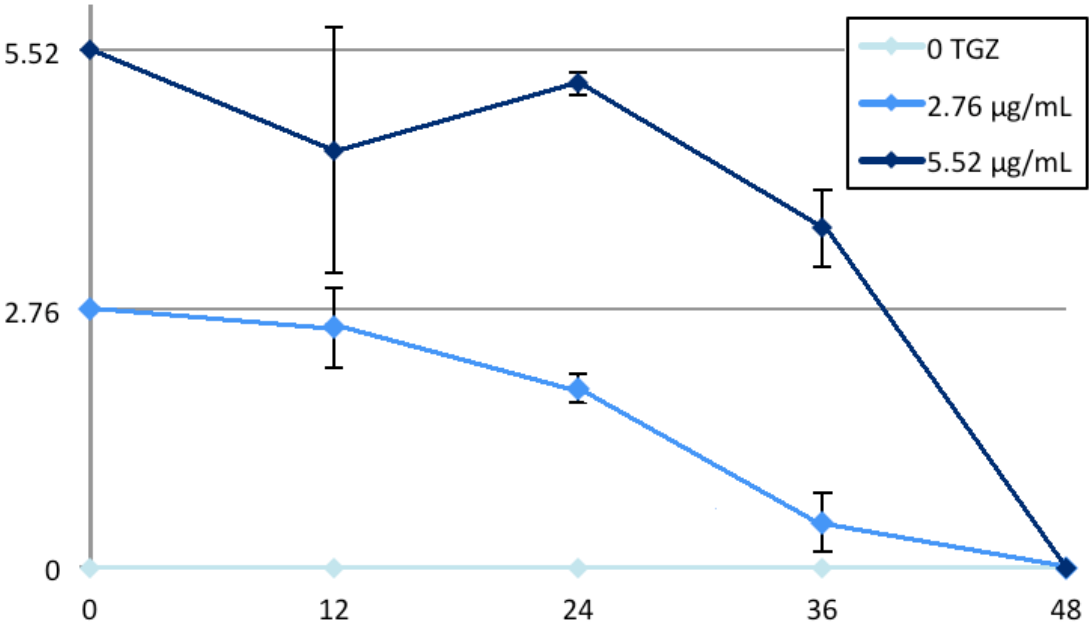

Figure 19: TGZ Consumption

Figure 19: TGZ consumption over time. The drug concentration in the medium is nearly constant for the first 24 hours, but then decreases to zero at 48 hours in all samples.

Discussion

The goal of these experiments was to correlate TGZ-induced cell stress with metabolic indicators that could be used to noninvasively and sensitively monitor the effects of the drug, e.g. in a microfluidic reactor. As expected, we found that high doses of TGZ can lead to outright toxicity. This is in agreement with the microfluidic

experiments (Figure 12), which showed that high doses of drug in excess of 0.25 mM clearly impact the viability of the cells. The decrease in culture DNA content correlated with significant alterations in the uptake or release of several amino acids (alanine, cysteine, glutamate, and glycine), which could serve as useful surrogate indicators of metabolic stress in HepG2 cells. It is worth investigating what nutritional deficiencies or health conditions might predispose a diabetic patient to abnormalities in the metabolism of these amino acids. Possibly, such compounded difficulties could be one contributing cause of idiosyncratic hepatoxicity of TGZ.

At lower, pharmacologically relevant dose, TGZ did not cause significant toxicity or alter the metabolism of amino acids. LC-MS analysis showed that the drug is completely consumed at 48 hrs, suggesting that the doses could be too low to cause a significant metabolic burden. Interestingly, TGZ consumptions did not occur until 24 hours, suggesting that the drug's metabolism requires enzymes that are induced, rather than constitutively expressed.

The analysis of TGZ drug derivatives remains elusive. Though they were previously detected (Kassahun et al. 2001), we were unable to repeat these results and detect the metabolic intermediates by LC-MS. One possible explanation is the difference in methodology for processing TGZ. Our studies use a HepG2 model with whole, living cells, while their model incubates the TGZ with human liver microsomes. It is possible that HepG2s do not express the full complement of xenobiotic transformation enzymes found in primary microsomes.

Chapter 5: Results for Metabolic Effects of Rosiglitazone and Metformin on HepG2 Cells in Well-Plate Culture

Examining the amount of DNA in each well is one way to look at the overall health of a HepG2 culture, as these cells tend to continue to proliferate even after they reach confluence, albeit more slowly. That is, healthy cultures should increase the cell number (and thus amount of DNA) over time. Our DNA data show that all cultures contained comparable amounts of DNA at 24 hours. However, at 48 hours, cultures treated with both drugs showed diminished growth. It is interesting to note that this effect correlates with dual-dosing rather than concentration of either drug dose. This suppressed cell growth suggests a drug interaction between metformin and ROSI. It could be shunting cell energy from growth and division to other metabolic pathways or reducing all functions of the cells, including growth.

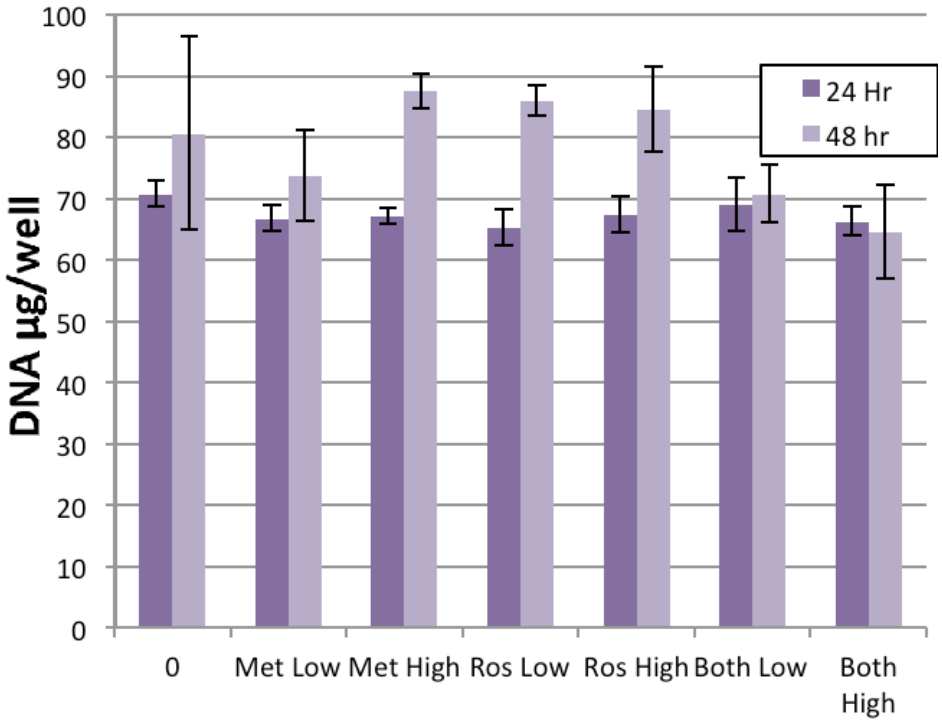

Figure 20: DNA Data After Treatment with Metformin and Rosiglitazone

Figure 20: DNA present is stable across all conditions at 24 hours, but at 48 hours, single-dose conditions show cell growth while cells dosed with both metformin and ROSI show no cell growth.

Both metformin and ROSI were detectable by LC-MS. While ROSI is consumed over time, metformin remains constant as it is not chemically metabolized by the liver (or any other organ).

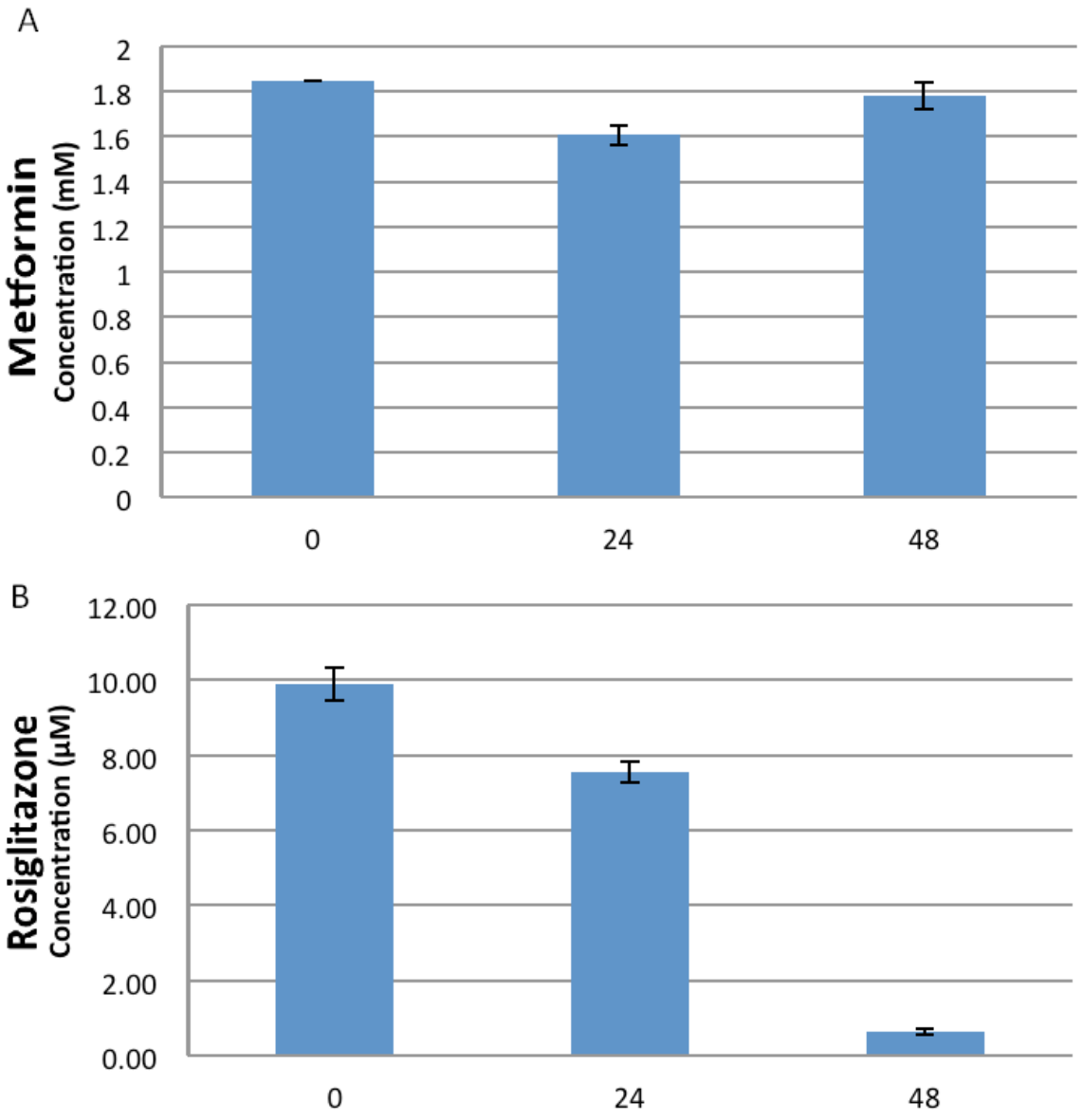

Figure 21: Metformin and Rosiglitazone Consumption

Figure 21: Metformin (A) and ROSI (B) concentration over a 48 hour time period. ROSI is consumed (metabolized by the hepatocytes) while metformin levels remain constant. Metformin is not metabolized by the liver or any other organ. It is excreted whole.

Lactate data is presented in two ways in figure 22. The first presentation, (A), shows lactate concentration in extracellular medium samples. This data offers a direct

comparison with glucose consumption. The second, (B), normalizes lactate produced over the observed period to the amount of DNA in each respective well. The data normalized to DNA accounts for the changes in cell growth over the 48 hour observation period. Unnormalized lactate data shows that metformin dominates an effect of lactate production suppression on each well. This effect is most obvious at high doses of metformin, regardless of the presence of ROSI. Type 2 ttest gives $p<0.01$ for all high doses of metformin when compared with the control.

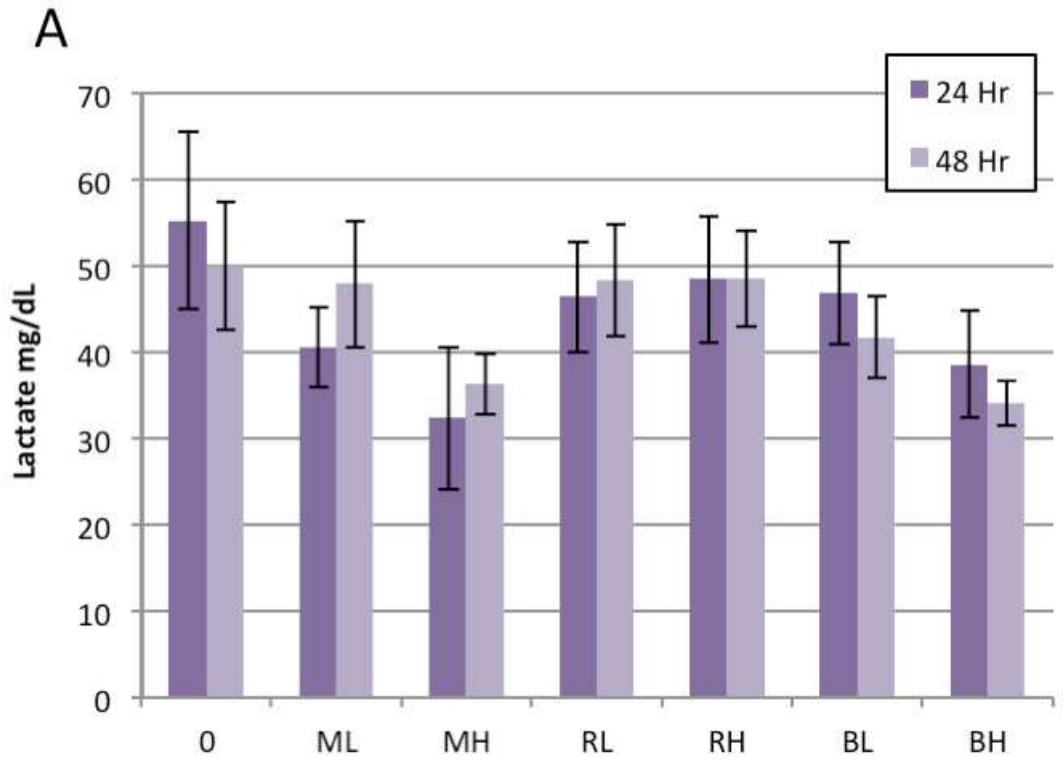
A
24 Hr
48 Hr
Lactate mg/dL
70
60
50
40
30
20
10
0
0
ML
MH
RL
RH
BL
BH

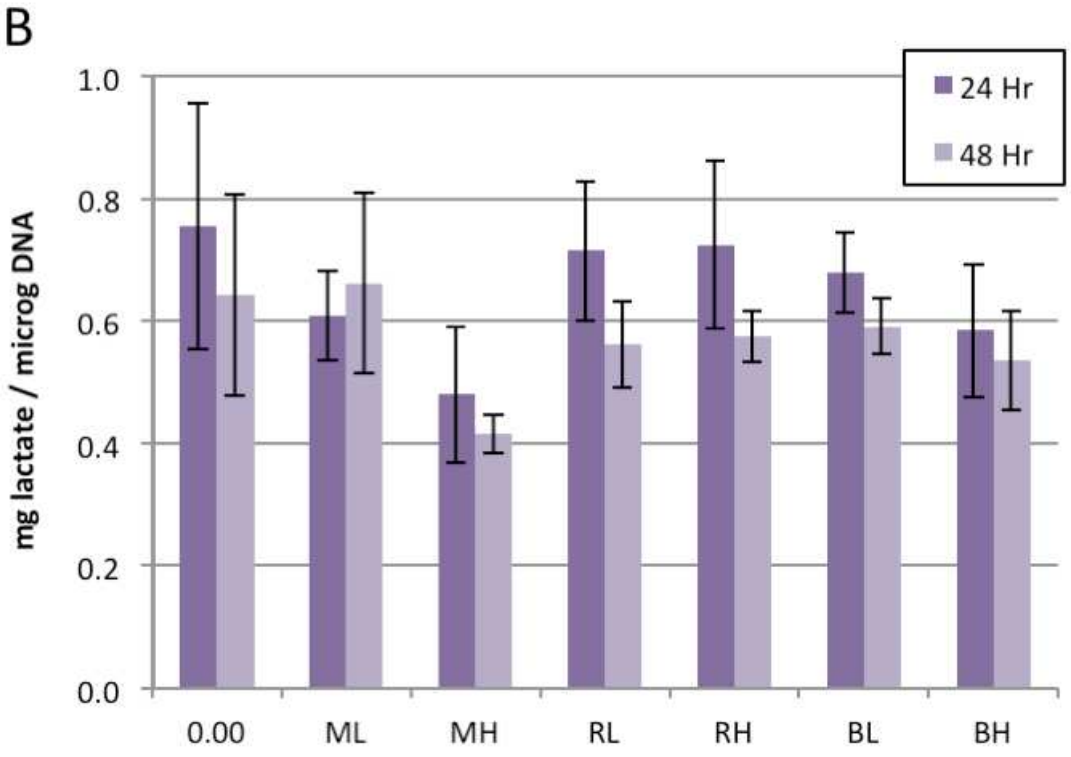
B
24 Hr
48 Hr
mg lactate / microg DNA
1.0
0.8
0.6
0.4
0.2
0.0
0.00
ML
MH
RL
RH
BL
BH

Figure 22: Lactate Data After Treatment with Metformin and Rosiglitazone

Figure 22: (A) Unnormalized actate concentrations in extracellular medium for each drug condition (see Table 1) (B) Lactate total amount normalized to DNA in each respective well. Error bars represent standard deviations among the 3 replicates for each condition.

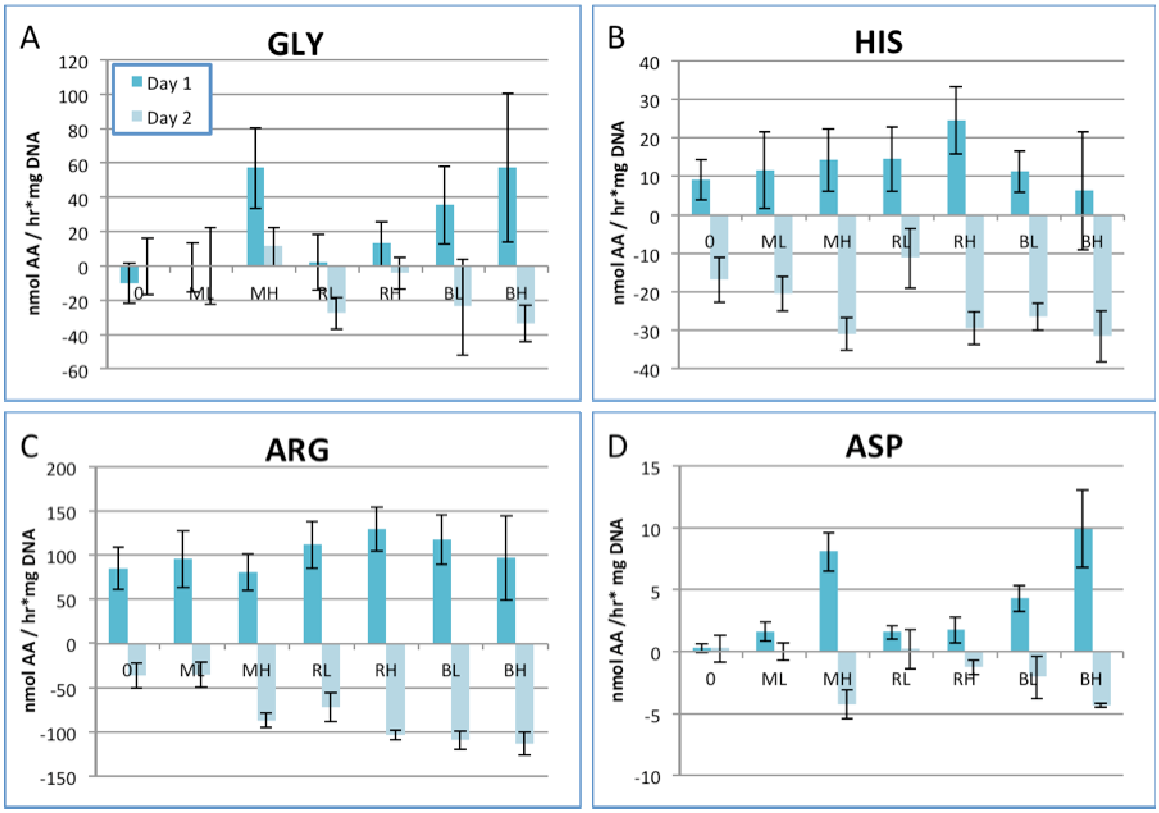

Figure 23: Amino Acids, Metformin Dominated Effects

Figure 23: The effects of these four amino acids, (A) Glycine (B) Histidine (C) Arginine (D) Asparagine, are dominated by the presence of metformin. Average hourly flux shown for day 1 and day 2. Day 1 fluxes are calculated from the differences in amino acid concentrations between samples taken at 24 hours and medium concentrations at time = 0. Day 2 data are calculated from difference in amino acid levels sampled at 48 hours and those sampled at 24 hours. In all cases, the conditions that differ the most from

the control on both day 1 (darker blue) and day 2 (light blue) are those conditions with high dosing of metformin, with or without the presence of ROSI. The presence of the ROSI appears to intensify the effects of metformin even at its low dose. While MH and BH conditions are similar in these examples, BL conditions tend to show exacerbated effects of metformin compared to low dosage of metformin alone (ML).

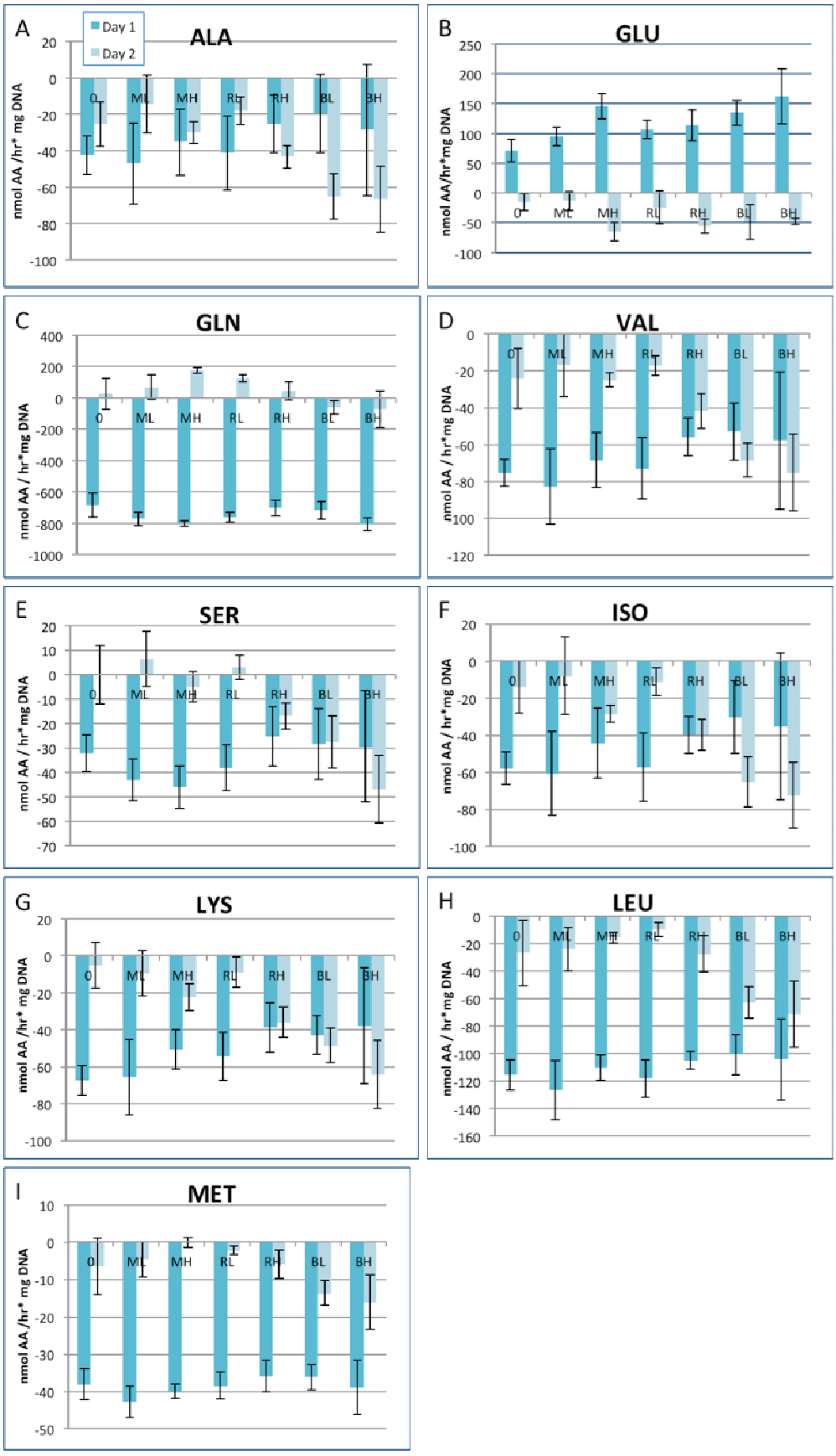
A
ALA
Day 1
Day 2
nmol AA /hr* mg DNA
B
GLU
nmol AA/hr*mg DNA
C
GLN
nmol AA / hr*mg DNA
D
VAL
nmol AA / hr*mg DNA
E
SER
nmol AA / hr*mg DNA
F
ISO
nmol AA / hr*mg DNA
G
LYS
nmol AA /hr* mg DNA
H
LEU
nmol AA / hr*mg DNA
I
MET
nmol AA /hr* mg DNA
0
ML
MH
RL
RH
BL
BH

Figure 24: Amino Acids, Drug Interaction Effects

Figure 24: These amino acids, (A) Alanine, (B) Glutamic Acid, (C) Glutamine, (D) Valine, (E) Serine, (F) Isoleucine, (G) Lysine, (H) Leucine,and (I)Methionine are affected most by dosing with both drugs. The conditions BL and BH differ most dramatically and consistently from the control conditions. Average hourly fluxes are shown for day 1 (dark blue) and day 2 (light blue). Positive values indicate amino acid production, and negative amino acid consumption.

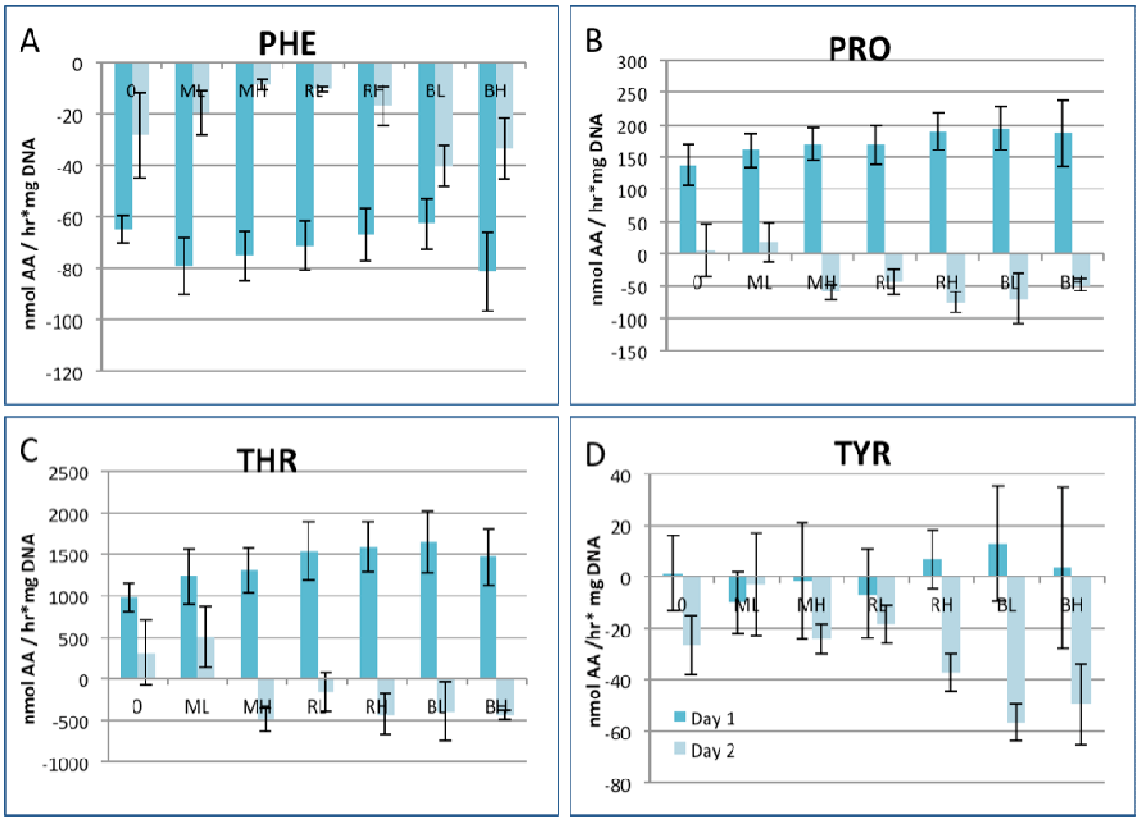

Figure 25: Amino Acids, Ambiguous Reactions

Figure 25: These amino acids, (A) Phenylalanine, (B) Proline, (C) Threonine, and (D) Tyrosine, show less clear relationship between drug dosage and production or consumption.

We attempted to detect metabolic energy cofactors ATP, ADP, NAD, NADH, NADP, NADPH by LC-MS. At the time of this data collection, sample prep methods remained incompatible with sensitive LC-MS protocols. Intracellular samples, obtained by sonication and vortex removal of solids, readily clogged the instrument, suppressing signal. Detection curves were inconsistent from run to run, often obscured by noise (data not shown). There were instances of detection for each of the six cofactors, but data was omitted because the method was deemed unreliable. Since this time, new methods of sample preparation and storage have been developed. Methanol extraction affords consistent and reliable detection of metabolic energy cofactors from whole cell samples while protecting the instrument from clogging.

Discussion

Examining the drug concentration data, it is interesting to note from figure 21 that ROSI (B) is completely consumed and broken down in the 48 hour experimental period while metformin concentration remains unchanged throughout (A). This is consistent with the unusual nature of metformin, a drug that acts despite being chemically unchanged by the body and excreted whole.

It appears from DNA data (figure 20) that while most of the HepG2 well culture populations continue to grow between the 24 hour and 48 hour time points, dual treatment with metformin and ROSI suppresses this colony growth. This indicates that the two drugs may combine to affect the cells differently than either drug alone.

Metformin has been associated with lactic acidosis, but the claims are disputed (Mistin et al. 1998 and 2004, Stades et al. 2004). There is some question as to whether

the metformin causes the overproduction of lactic acid, or whether the patients who experienced this rare side effect were simply under other stressors like heart disease. We expected to see high levels of lactate production in all of the metformin treated samples, however the data show (Figure 22) the opposite. Samples treated with high doses of metformin express lower levels of lactate productions regardless of ROSI concentration. In figure 22 A, it is clear that the lactate produced by the cells is produced within the first 24 hours of the experiment. Levels remain more or less constant after that, with metformin treated samples producing a little bit more lactate over the second day of drug exposure, and those treated with both ROSI and metformin consuming a little bit of lactic acid over the second 24-hour period.

Amino acid data suggest some interesting effects of drug dosing on HepG2 cells. Alanine(Figure 24 A), glycine (Figure 23 A), and serine (Figure 24 E) are all amino acids that are consumed in the production of pyruvate. (Diwan, 1998) All three of these amino acids are most heavily consumed under the high dose combination drug treatment (BH). Alanine and serine show the same relationship, being consumed overall and consumed most heavily in the second day of treatment with the combination of metformin and ROSI. When the cells are in a starved state, they produce their own glucose from gluconeogenesis, building the simple sugar from lactate and pyruvate. The main source of pyruvate in this process is amino acids like Alanine and serine. These amino acid results indicate that the cells may be shifting more energy to gluconeogenesis when treated with both drugs simultaneously. This effect appears on the second day of treatment compared to the control, which has higher levels of consumption in the first

day of treatment but lower levels of amino Alanine and serine consumption overall. A similar pattern can be observed for valine, isoleucine, and lysine.

This analysis suggests more questions than answers. The behavior of the cells in the first 24 hours is not informative. The HepG2 cells produce much lactate very quickly, regardless of treatment, and this behavior may be masking some important subtler shifts that occur in the later hours of drug exposure – when most of the ROSI is being metabolized by the cells. Decoupling the initial lactate production from our observations of drug treatment may help. Additionally, it would be very helpful to have quantified data for metabolic energy cofactors ATP, ADP, NAD, NADH, NADP, and NADPH. We were unable to access that information from these experimental samples. The energy currency of the cell would give more meaning to the changes in amino acid concentration over time. Fortunately, we have since developed sample preparation methods that are more compatible with LC-MS and we have improved our LC-MS detection methods for these compounds, so it is likely that this data could be extracted from future HepG2 studies in our lab. With this in mind, a second experiment was designed in collaboration with Gautham Sridharan. In this experiment, some HepG2 wells were pretreated with drug in order to get them through the first 24 hour push for lactate formation before starting a 48 hour experiment. The experiment is outlined in Table 3, below:

Condition		0 hrs	24 hrs	48 hrs	72 hrs
A	Control	No Drug	Collect		
B	Control	No Drug	No Drug	Collect	
C	Control	No Drug	No Drug	No Drug	Collect
D	Pre-treat Met	Metformin	Collect		
E	Pre-treat Met	Metformin	Met and Rosi	Collect	

F	Pre-treat Met	Metformin	Met and Rosi	Met and Rosi	Collect
G	No Metformin	No Drug	Rosi	Collect	
H	No Metformin	No Drug	Rosi	Rosi	Collect

Table 3: Outline of HepG2 experiment. Two pre-treated conditions are shown at 0 hrs, either plain high glucose DMEM, or high glucose DMEM with metformin added (2 mM). At 24 hours, one sample each of control conditions and metformin pre-treated condition was collected. Medium was saved and stored and cells were lifted and stored as described in previous experimental method sections. Medium from all other wells was stored and replaced with fresh medium of one of the following conditions: no drug, ROSI (10 µM), or metformin and ROSI (2 mM and 10µM respectively).

This experiment makes it easy to measure the effect of drug dosing on metabolic fluxes rather than straight concentration. This is an improvement on the previous experiment reported in this chapter because it allows access to actual *before* and *after* values of metabolite concentration rather than requiring a well-to-well comparison for determining fluxes. These new fluxes will be true fluxes and not merely estimates.

This experiment also decouples the first 24 hours of reaction to drug from the first 24 hours of reaction to fresh medium. Thus, the effect of the drug treatment and drug combination therapy on the hepatocytes can be more meaningfully analyzed. This experiment is still in progress and will not be completely covered in this thesis. The experiment has to be re-run to add another data point: the condition of pre-treated metformin and sustained treatment with metformin to help illustrate what drug effects are caused by metformin alone, and whether there is a significant drug interaction between metformin and ROSI.

Despite the incomplete nature of this experiment, the lactate data, shown below, indicate that metformin increases the portion of glucose directed to lactate production to maximal levels regardless of exposure time. One glucose molecule can be used to produce two lactatic acid molecules, and that is the ratio attained via metformin exposure (D,E,F). ROSI treatment by itself (G,H) suppresses lactate production as compared to the control (A,B,C). Lactate can also come from pyruvate, which can be produced by several amino acids (Alanine, cysteine, glycine, serine, and threonine).

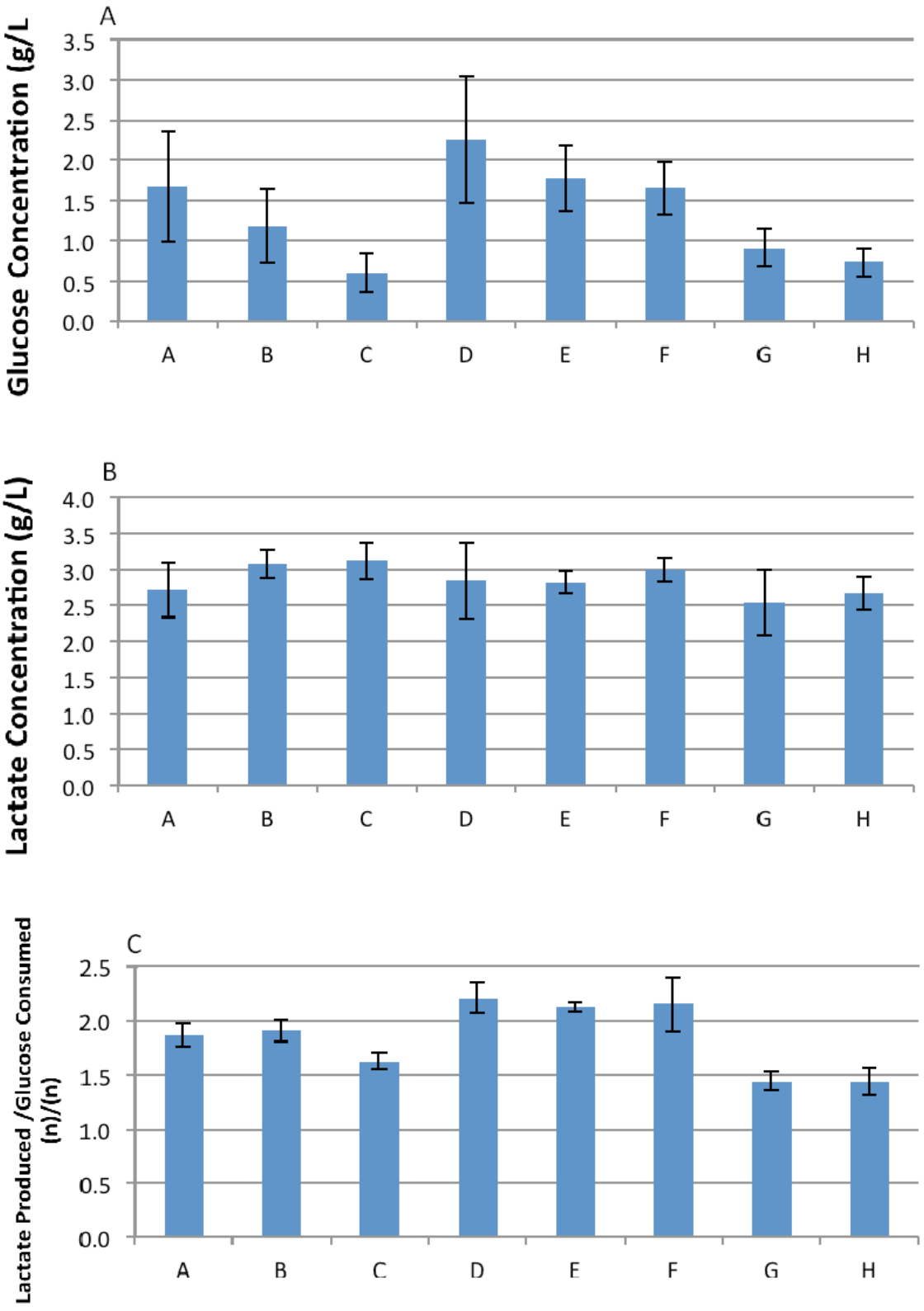

Figure 26: Preliminary Data: Glucose and Lactate

Figure 26: Glucose consumption (A) and lactate production (B) for HepG2 cells. (C) Lactate produced compared to glucose consumed. Conditions A through H correspond to Table 3. Initial glucose concentration in DMEM is 4.5 g/L. A B C

When the rest of this data is analyzed with the methods Michael Yi and Gautham Sridharan are developing, we expect to see amino acid and cofactor levels consistent with the production of lactic acid in the metformin treated samples.

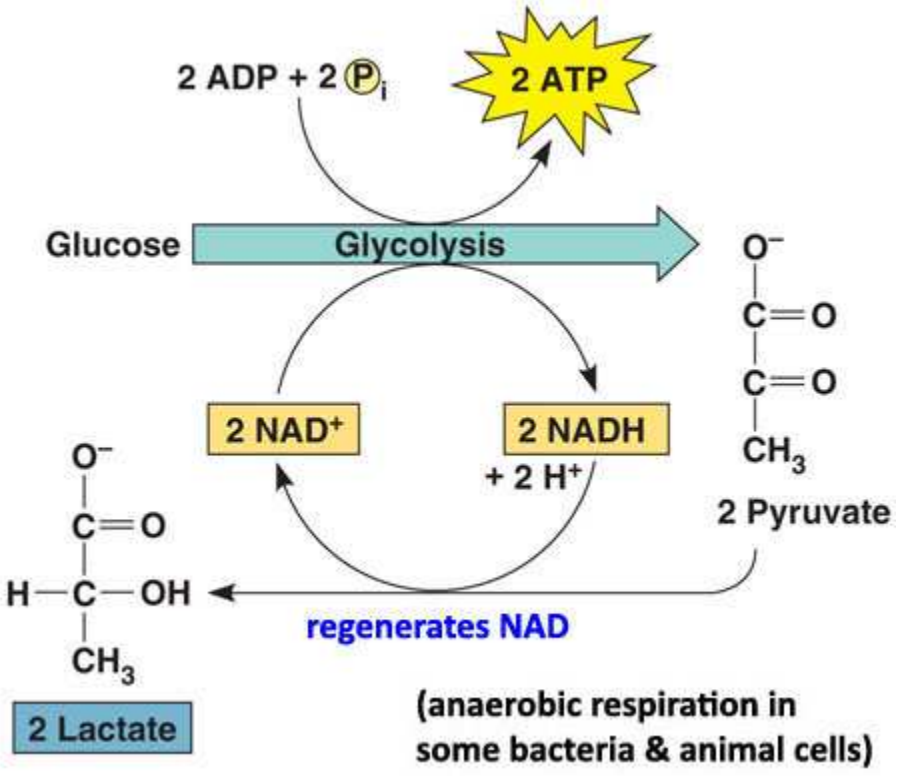

Figure 27: Lactic Acid Fermentation

Figure 27: Lactic acid fermentation (Cummings, 2011)

$$C_6H_{12}O_6 + 2NAD^+ + 2ADP + 2Pi \leftrightarrow 2C_3H_4O_3 + 2ATP - 2NADH + 2H^+$$

$$C_3H_4O_3 + NADH \leftrightarrow NAD^+ + C_3H_6O_3$$

Lactic acid is produced from pyruvate with the help of NADH. We may expect to see an elevated ratio of ATP:ADP but low NADH:NAD ratio in the cofactors, and we may also expect to see reduced amounts of alanine, cysteine, glycine, serine, and threonine which can produce pyruvate.

Antidiabetic compounds metformin and ROSI were tested on HepG2 cells in traditional well plate culture. A LC-MS method was developed to quantify the concentrations of both drugs in the cell culture medium. As expected, ROSI was consumed within 48 hours while metformin levels remained. DNA results suggest that this combinatorial therapy may hinder cell proliferation during the experimental period. Amino acid fluxes were analyzed and show some differences based upon exposure to drugs. Two main patterns emerged: metformin-dominated response or drug interaction response. Though this is interesting, another experiment (proposed above) is needed to measure these affects more meaningfully. The preliminary data from this experiment shows elevated utilization of glucose for lactate production in metformin-treated samples. In conjunction with improved sample preparation and energy cofactor analysis LC-MS methods, this experiment should elucidate the relationship between metformin and ROSI impact on HepG2 metabolism, possibly illuminating metabolic indicators of cell stress.

General Discussion

In this research, we developed a microfluidic reactor for the culture of HepG2 cells and the establishment of a diffusion gradient over the cells. We demonstrated cell culture on the order of weeks. We established a steady state diffusion gradient of dye,

drug, and fluorescent probe. We used this reactor to expose HepG2 cells to highly predictable and controllable concentrations of the antidiabetic drug TGZ, which is known to cause idiosyncratic liver failure in a subset of in vivo patients. Some cells were exposed at very toxic levels while other cells were exposed at lower levels. Cellular damage conformed to the steady state diffusion gradient of TGZ within the cell culture chamber. Cells subjected to high concentrations of TGZ (> 0.25 mM) were killed while cells exposed to lower concentrations survived.

Traditional well plate experiments were run with TGZ to mine for metabolic indicators of stress. Metformin and ROSI were also studied, with an interest in drug interactions. Two patterns emerged: metformin domination and drug interaction. Glucose use for lactate production, for instance, is metformin dominated while HepG2 cell proliferation is suppressed by the combined effect of both drugs.

Novel methods were developed for studying the effects of antidiabetic compounds on HepG2 cells. Drug concentration was quantified with LC-MS in extracellular medium for all drugs used. Conjugated intermediates were sought but not detected, and energy cofactors ATP, ADP, NAD, NADH, NADP, and NADPH were detected, but it was found that methanol extraction is needed for sample preparation for the cell fractions to be used in LC-MS.

Here we have designed and implemented a reactor that holds potential for examining drug effects on the liver in new and sensitive ways. A diffusion gradient establishes a wide variety of conditions over a large number of cells at the same time. Many concentrations or drug interactions can be studied on a single chip adding

efficiency to the advantages of a more physiologically relevant *in vitro* platform. We have simultaneously developed LC-MS methods of analysis that increase the depth of our understanding of HepG2 drug metabolism. Such methods may elucidate subtle details and indicators of drug toxicity on the liver. This promises to open up a great amount of information about cell function in response to nutrient or drug treatment in a manageable number of experiments.

Chapter 5: Future Work

This research sets a foundation for the development of further, more sensitive exploration of HepG2 metabolism in microfluidic culture with a long-term goal to understand the metabolic basis of idiosyncratic hepatoxicity, in particular toxic effects caused by drug-drug interaction. Deeper investigation by traditional well plate experiments and metabolic modeling will indicate markers of cell stress (for instance, ATP:ADP or NAD:NADH ratios). Developing optical methods of detection for such indicators of cellular metabolism within the microfluidic realm will vastly increase our options for *in vitro* drug testing . Our group's work to optimize the measurement of these cofactors by developing a consistent and accurate LC-MS method of detection is one step in the process. Gautham Sridharan's work to develop a robust and comprehensive computer model of HepG2 metabolism is another powerful tool towards a more complete understanding of drug metabolism and its effects on the liver.

Some promising work from collaborators suggests that some cofactors may be quantifiable via confocal microscopy. The combination of a more thorough understanding of the metabolic workings of HepG2 cells under drug treatment (from traditional experimentation, new methods for metabolite detection, and robust models)

and an optical means of measuring metabolic cofactors could combine to make the microfluidic reactor described here a very sensitive and powerful drug testing platform. Such a combination of methods and information will expand our understanding of cell function in the presence of antidiabetic drugs and will improve our ability to test these drugs safely and effectively before they are released to market. It is even possible that a technology like this one could help determine what subset of patients might experience adverse drug interactions. If high risk groups could be separated from low risk groups, it would save life and health for those at high risk, allow low risk patients access to drug therapy they need, and help to support pharmaceutical innovation and industry. It could be an advantageous end to both patients and business.

To reach this goal, we must develop a more reliable way to test for our indicators, a thorough understanding of the metabolic implications of drug treatment, and reproducible optical means of accessing this information from cells in microfluidic culture.

References

American Diabetes Association.*Standards of Medical Care in Diabetes – 2009*doi: 10.2337/dc09-S013 *Diabetes Care January 2009 vol. 32 no. Supplement 1 S13-S61*
Atencia, J., Morrow, J., and Locascio, L.E. The microfluidic palette: a diffusive gradient generator with spatio-temporal control. Lab Chip 9, 2707, 2009.

Berthiaume F, Moghe PV, Toner M, Yarmush ML. Effect of extracellular matrix topology on cell structure, function, and physiological responsiveness: hepatocytes cultured in a sandwich configuration. FASEB J. 1996 Nov;10(13):1471-84.

Carraro, Amedeo. Hsu, Wen-Ming. Kulig, Katherine. Cheung, Wing. Miller, Mark. Weinberg, Eli. Swart, Eric. Kaazempur-Mofrad, Mohammad. Borenstein, Jeffrey. Vacani, Joseph. In vitro analysis of a hepatic device with intrinsic microvascular-based channels. Biomedical Microdevices. 2008. Volume 10, Number 6, 795-805, DOI: 10.1007/s10544-008-9194-3

Centers for Disease Control and Prevention.*National diabetes fact sheet: national estimates and general information on diabetes and prediabetes in the United States, 2011*. Atlanta, GA: U.S.
Cohen, Barbara Janson; Wood, Dena Lin; Memmler, Ruth Lundeen, Cohen, Daniel James. Memmler's The Human Body in Health and Disease, 9th Edition. Lippincott Willipams& Wilkins. 1999. ISBN-13: 9780781721103

Cohen, S. A., De Antonis, K. M., Applications of amino acid derivatization with 6-aminoquinolyl-N-hydroxysuccinimidyl carbamate. Analysis of feed grains, intravenous solutions and glycoproteins. *J Chromatogr A* 1994, *661*, 25-34.

Cohen, S.A., and De Antonis, K.M. Applications of amino acid derivatization with 6-aminoquinolyl-N-hydroxysuccinimidyl carbamate. Analysis of feed grains intravenous solutions and glycoproteins. J Chromatogr A 661, 25, 1994

Cummings, Benjamin. Lactic Acid Fermentation. Pearson Education. http://kentsimmons.uwinnipeg.ca/cm1504/pyruvate.htm. 2011

Dennis. Wang, Regina. Doss, George. Baillie, Thomas. Studies on the metabolism of troglitazone to reactive intermediates in vitro and in vivo. Evidence for novel biotransformation pathways involving quinone methide formation and thiazolidinedione ring scission. Chemical Research in Toxicology. (14) 62-70. 2001.

Department of Health and Human Services, Centers for Disease Control and Prevention, 2011.

Diwan, Joyce. Gluconeogenesis and Amino Acid Catabolism: Carbon Skeletons.

Food and Drug Administration. FDA Briefing Information, AVANDIA (Rosiglitazone Maleate) Tablets, for the July 13-14, 2010 Joint Meeting of the Endocrinologic and Metabolic Drugs Advisory Committee and Drug Safety and Risk Management Advisory Committee (PDF –24MB). http://www.fda.gov/AdvisoryCommittees/CommitteesMeetingMaterials/Drugs/EndocrinologicandMetabolicDrugsAdvisoryCommittee/ucm218491.htm . 2010

Gale, E. A.: Lessons from the glitazones: a story of drug development. *Lancet*, **357**: 1870-1875 (2001).

Gillies CL, Abrams KR, Lambert PC, et al. Pharmacological and lifestyle interventions to prevent or delay type 2 diabetes in people with impaired glucose tolerance: systematic review and meta-analysis. *BMJ* 2007; 334 (7588): 299

Graham, D. J., Green, L., Senior, J. R. and Nourjah, P.: Troglitazone-induced liver failure: a case study. *Am. J. Med.*, **114**: 299-306 (2003).

Grattagliano, I., Bonfrate, L., Diogo, C. V., Wang, H. H., *et al.*, Biochemical mechanisms in drug-induced liver injury: certainties and doubts. *World J Gastroenterol* 2009, *15*, 4865-4876.

Gripon, P., Rumin, S., Urban, S., Le Seyec, J., *et al.*, Infection of a human hepatoma cell line by hepatitis B virus. *Proc Natl Acad Sci U S A* 2002, *99*, 15655-15660.

Hart, S. N., Li, Y., Nakamoto, K., Subileau, E. A., *et al.*, A comparison of whole genome gene expression profiles of HepaRG cells and HepG2 cells to primary human hepatocytes and human liver tissues. *Drug Metab Dispos*, *38*, 988-994. 2010.
http://rpi.edu/dept/bcbp/molbiochem/MBWeb/mb1/part2/gluconeo.htm and
http://rpi.edu/dept/bcbp/molbiochem/MBWeb/mb2/part1/aacarbon.htm 1998.

Hundal R, Krssak M, Dufour S, Laurent D, Lebon V, Chandramouli V, Inzucchi S, Schumann W, Petersen K, Landau B, Shulman G (2000). *Mechanism by which metformin reduces glucose production in type 2 diabetes. Diabetes***49** (12): 2063–9. doi:10.2337/diabetes.49.12.2063. PMID 11118008

Hundal, Ripudaman. Krssak, Martin. Dufour, Sylvie. Laurent, Didier. Lebon, Vincent. Chandramouli, Visvanathan. Inzucchi, Silvio. Schumann, William. Petersen, Kitt. Landau, Bernard. Shulman, Garald. Mechanism by which metformin reduces glucose production in type 2 diabetes. Diabetes. Vol 49. 2000.

International Diabetes Federation.IDF Atlas.http://www.diabetesatlas.org 2010.

Jaeschke, Hartmut. Troglitazone hepatoxicity: are we getting closer to understanding

idiosyncratic liver injury? Toxicological Sciences. (97)1:1-3 2007.

Jones, Julie R. Barric, Cordelia. Kim, Kyoung-Ah. Linder, Jill. Blondeau, Bertrand. Fujimoto, Yuka. Shiota, Masakazu. Kesterson, Robert A. Kahn, Barbara B. Magnuson, Mark A. Deletion of PPARγ in adipose tissue of mice protects against high fat diet-inducing obesity and insulin resisance. PNAS. 2005.

Kalem Kassahun, Pail Pearson, Wei Tang, Ian McIntosh, Kwan Leung, Charles Elmore, Dennis Dean, Regina Wang, George Doss, and Tomas A Baillie. Studies on the metabolism of troglitazone to reactive intermediates in vitro and in vivo. Evidence for novel biotransformation bathways involving quinone methide formation and thiazolidinedione ring scission. Chem. Res. Toxicol. 2001 (14) 62-70.

Kaplowitz N. Idiosyncratic drug hepatoxicity. Nat. Rev. Drug Discov. 2005;4:489-499.

Kassahun, Kelem. Pearson, Paul. Tang, Wei. McIntosh, Ian. Leung, Kwan. Elmore, Charles, Dean, Studies on the metabolism of troglitazone to reactive intermediates in vitro and in vivo. Evidence for novel biotransformation pathways involving quinone methide formation and thiazolidinedione ring scission. Chem Res Toxicol. 2001 Jan;14(1):62-70.

Kirpichnikov, Dmitri, FcFarlane, Samy. Sowers, James. Metformin: an update. Annals of Internal Medicine. 137(1):25-33. 2002

Lawrence E. Barker, PhD, Karen A. Kirtland, PhD, Edward W. Gregg, PhD, Linda S. Geiss, MA, and Theodore J. Thompson, MS. Geographic distribution of diagnosed diabetes in the United States: a diabetes b. *American Journal of Preventive Medicine* 2011;40(4)

Leclerc, Eric. Sakai, Yasuyuki. Fujii, Teruo. Cell Culture in 3-Dimensional Microfluidic Structure of PDMS (polydimethylsiloxane) Biomedical Microdevices. Volume 5, Number 2, 109-114, DOI: 10.1023/A:1024583026925. 2003

Loomis, M. E., An enzymatic fluorometric method for the determination of lactic acid in serum. *J Lab Clin Med* 1961, *57*, 966-969.

Ma, Bo. Zhang, Guohao. Quin, Jianhua. Lin, Bingcheng. Characterization of drug metabolites and cytotoxicity assay simultaneously using an integrated microfluidic device. Lab Chip, 2009, 9:232-238

Masubuchi, Yasuhiro. Metabolic and non-metabolic factors determining troglitazone hepatoxicity, a review. Drug Metab Pharmacokinet. 21 (5) 347-356 2006

Matthieu, Jean. Briffault, Anne-Sophie. Letourneur, Franck. Chafey, Philippe. Merlier, Franck. Grandvalet, Yves. Legallais, Cecile. Leclerc, Eric. Integrated Proteomic and Transcriptomic Investigation of the Acetaminophen Toxicity in Liver Microfluidic

Biochip. PLoS One. 2011; 6(8): e21268.

Misbin RI, Green L, Stadel BV, Gueriguian JL, Gubbi A, Fleming GA*: Lactic acidosis in patients with diabetes treated with metformin. N Engl J Med 338:265–266, 1998*

Misbin RI*: The phantom of lactic acidosis due to metformin in patients with diabetes. Diabetes Care 27:1791–1793, 2004*

Nalayanda DD, Puleo CM, Fulton WB, et al. Characterization of pulmonary cell growth parameters in a continuous perfusion microfluidic environment. Exp Lung Res. 2007;33:321–335

Nerstedt, A. Johansson, A. Andersson, C.X. Cansby, E. Smith, U. Mahlapuu, M. AMP-activated protein kinase inhibits IL-6-simulated inflammatory response in human liver cells by suppressing phosphorylation of signal transducer and activator of transcription 3 (STAT3). Diabetologia. 2010. 53:2406-2416.

Nissen, Steven E. Wolski, Kathy. Effect of rosiglitazone on the risk of myocardial infarction and death from cardiovascular causes. New England Journal of Medicine. 356:2457-2471. 2007.
O'Brien, P. J., Irwin, W., Diaz, D., Howard-Cofield, E., *et al.*, High concordance of drug-induced human hepatotoxicity with in vitro cytotoxicity measured in a novel cell-based model using high content screening. *Arch Toxicol* 2006, *80*, 580-604.

Rachek, LI. Yuzefovych, LV. Ledoux, SP. Julie NL, Wilson, GL. Troglitazone, but not rosiglitazone, damages mitochondrial DNA and induces mitochondrial dysfunction and cell death in human hepatocytes. Toxicol Appl Pharmacol. 2009; 240(3):348-54.

Schutte, J. Hagmeyer, B. Holzner, F. Kubon, M. Werner, S. Freudigmann, C. Benz, K. Bottger, J. Gebhardt, R. Becker, H. Stelzle, M. "Artificial micro organs"--a microfluidic device for dielectrophoretic assembly of liver sinusoids. Biomed Microdevices. 2011 Jun;13(3):493-501.

Si, Y., Yoon, J., and Lee, K. Flux profile and modularity analysis of timedependent metabolic changes of de novo adipocyte formation. Am J Physiol Endocrinol Metab 292, E1637, 2007

Stades AME, Heikens JT, Erkelens DW, Holleman F, Hoekstra JBL*: Metformin and lactic acidosis: cause or coincidence? A review of case reports. J Int Med 255:179–187, 2004*

Sung, Jong Hwan. Shuler, Michael L. A micro cell culture analog (μCCA) with 3-D hydrogel culture of multiple cell lines to assess metabolism-dependent cytotoxicity of anti-cancer drugs. Lab Chip, 2009 9, 1385-1394.

Tafazoli, S., Spehar, D.D. and O'Brien, P.J. (2005) Oxidative stress mediated

idiosyncratic drug toxicity, Drug Metab Rev, 37, 311-325.

Thibodean, Patton. The Human Body in Health and Disease.3rd Edition. Mosby. 2002.

Towler, Mhairi. Hardie, Grahame. AMP-activated protein kinase in metabolic control and insulin signaling. Circulation Research. 2007; 100:328.

Trinder, P., Determination of blood glucose using an oxidase-peroxidase system with a non-carcinogenic chromogen. *J Clin Pathol* 1969, *22*, 158-161.

Van Midwould, Paul. Merema, Marjolijn. Verpoorte, Elisabeth. Groothuis, Geny. A microfluidic approach for *in vitro* assessment of interorgan interactions in drug metabolism using intestinal and liver slices. Lab Chip 2010, 10, 2778-2786.

Watkins, P. B. and Whitcomb, R. W.: Hepatic dysfunction associated with troglitazone. *N. Engl. J. Med.*, **338**: 916-917 (1998).

Whitesides, G.M., Ostuni, E., Takayama, S., Jiang, X., and Ingber, D.E. Soft lithography in biology and biochemistry. Annu Rev Biomed Eng 3, 335, 2001.

Whitesides. The origins and the future of microfluidics. Nature. vol 442. 2006.

Wild S, Roglic G, Green A, Sicree R, King H. *Global prevalence of diabetes: estimates for the year 2000 and projections for 2030*. Diabetes Care. 2004 May;27(5):1047-53.

Wilkening, S. Stahl, F. Bader, A. Comparison of primary human hepatocytes and hepatoma cell line HepG2 with regard to their biotransformation properties. Drug Metab Dispos. 2003 Aug;31(8):1035-42.

Xuemei Liao, Yanfei Wang, Chi-Wai Wong. Troglitazone induces cytotoxicity in part by promoting the degradation of peroxisome proliferator-activated receptor γ co-activator-1α protein. British Journal of Pharmacology. Volume 161, Issue 4, pp 771-781. October 2010.

Yamamoto, Y., Yamazaki, H., Ikeda, T., Watanabe, T., *et al.*, Formation of a novel quinone epoxide metabolite of troglitazone with cytotoxicity to HepG2 cells. *Drug Metab Dispos* 2002, *30*, 155-160.

Ye, Nannan. Qin, Jianhua. Shi, Weiwei. Liu, Xin. Lin, Bingcheng. Cell-based high content screening using an integrated microfluidic device. ***Lab Chip***, 2007, **7**, 1696-1704 **DOI:** 10.1039/B711513J

Yki-Jarvinen, Hannele. Thiazolidinediones. New England Journal of Medicine. 2004; 351:1106-1118.